III. R & D RELATED TO A FUTURE RARE ISOTOPE ACCELERATOR FACILITY

OVERVIEW

The Rare Isotope Accelerator (RIA), a next-generation facility for basic research in nuclear physics, is a high priority for construction in the United States by the Department of Energy. The overall concept for RIA was developed during 1999 by the ISOL Task Force, a sub-committee of the Nuclear Science Advisory Committee (NSAC). A preliminary cost analysis of the RIA project was developed jointly by Argonne National Laboratory and the National Superconducting Cyclotron Laboratory of Michigan State University. The costs were reviewed by another subcommittee of NSAC in January, 2001. Based on this analysis and review the estimated construction cost (TEC) for RIA is $644M in year 2001 dollars. It is possible that construction of RIA could begin in 2005 following various preliminary decisions and site selection. In the meantime, to prepare for construction on this time scale it is essential to continue a vigorous R&D program for RIA. This section is a progress report on the RIA R&D efforts at Argonne.

The RIA R&D topics addressed at Argonne during the year 2001 fall under four main categories: Heavy-ion Linac Technology, RIA Beam Dynamics, and Rare Isotope Production, Separation and Diagnostics, sections A-C below.

We have continued to develop and improve the baseline design for the RIA proposal. Highlights of developments during 2001 include:

- Successful operation of a prototype 345 MHz superconducting resonator continuously for 28 days at 7 MV/m accelerating gradient.
- Development of methods to refine drift-tube resonator designs to compensate for beam steering effects that are inherent in certain quarter-wave resonators.
- Extensive refinements of the beam dynamics simulations and improvements to the lattice of the RIA Driver Linac.
- Development of a novel new RFQ structure, called the hybrid-RFQ, to greatly improve the efficiency of the initial post-acceleration of radioactive species up to mass 240 from the 1+ charge state.

- Successful development of a bunch shape monitor with 20 psec resolution for heavy ions.

- Completion of the design of a novel adjustable-thickness, liquid-lithium target for use with heavy ion beams up to 4 kW for in-flight fragmentation at the NSCL A1900 fragment separator.

A. HEAVY-ION LINAC TECHNOLOGY

a.1. Superducting RF: Prototype Superconducting Drift-Tube Cavities (K. W. Shepard, Joel Fuerst, Michael Kelly, and Mark Kedzie)

Three drift-tube cavities (Fig. III-1) covering a velocity range of $0.12 < v/c < 0.6$ are being developed for the RIA driver linac. Preliminary designs for a 115 MHz quarter-wave (QWR) cavity and a 172.5 MHz half-wave (HWR) cavity have been completed. The design of a two-spoke 345 MHz cavity for RIA has been completed and construction of a niobium prototype has begun. Figure III-2 shows the niobium end-cap assembly for the two-spoke prototype cavity.

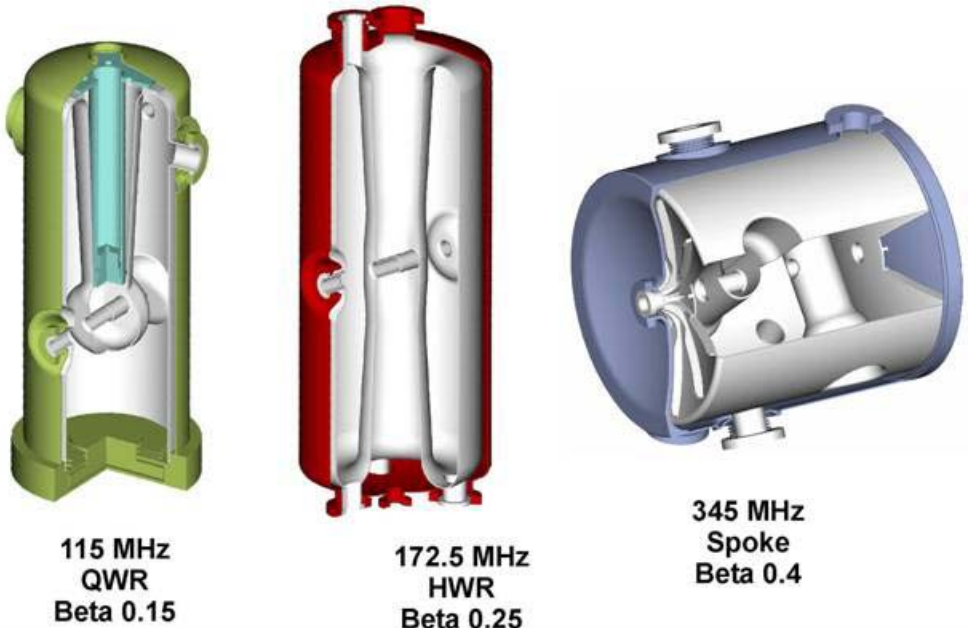

Fig. III-1. Cut-away section views of the niobium shell and stainless-steel housing of three drift-tube loaded cavities for the RIA driver linac

Fig. III-2. Niobium end-cap assembly for the prototype two-cell cavity after welding.

a.2. Superconducting RF: Test Facility Expansion (K. W. Shepard, Joel Fuerst, Michael Kelly, and Mark Kedzie)

The prototype 2-cell spoke cavity does not fit the vertical test cryostats located in the existing shielded test area. A new cryostat has been designed to permit testing the 2-cell spoke cavity with separate cavity and

cryogenic vacuum systems. This will enable development of procedures to reduce particulate contamination of the cavity and increase operating field levels. The new cryostat (shown in Fig. III-3) can be extended to permit future installation of a focusing/steering magnet adjacent to the resonator for possible tests with beam. Figure. III-4 shows the cryostat installed in a new resonator test cave constructed with a shield wall of high density concrete blocks.

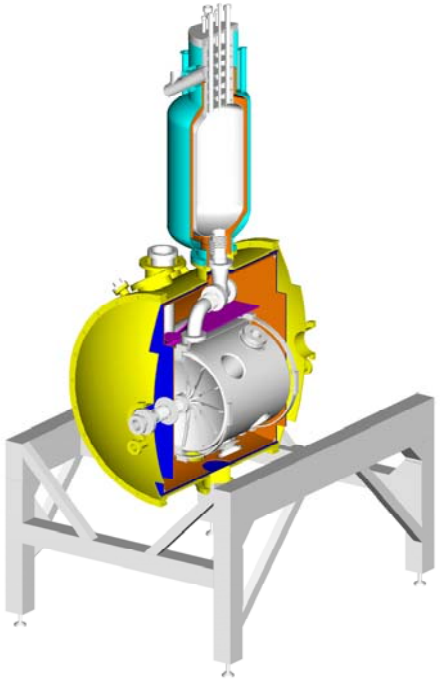

Fig. III-3. Horizontal cryostat assembly.

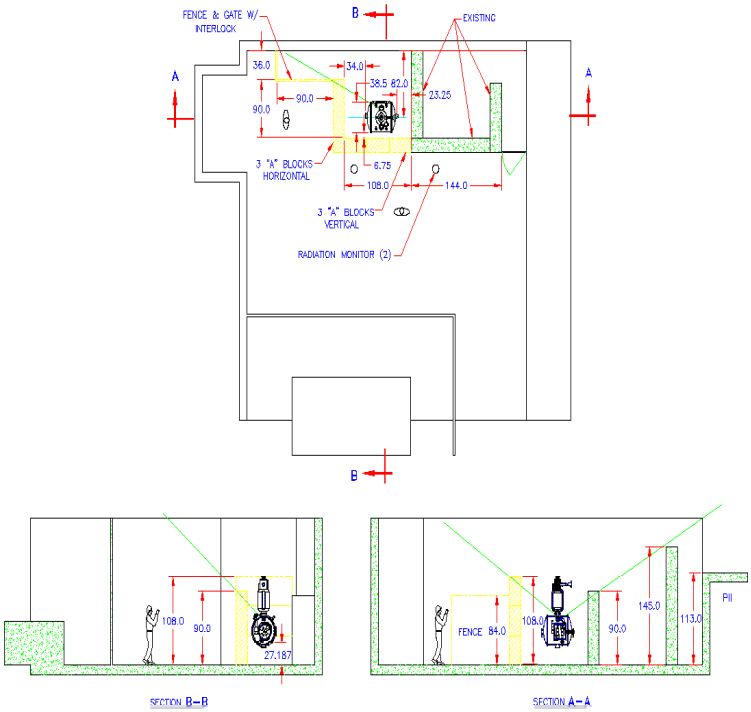

Fig.III- 4. Layout of new resonator test cave.

a.3. **Superconducting RF: Steering Effects in Quarter-Wave Cavities** (K. W. Shepard, Joel Fuerst, Michael Kelly, and Mark Kedzie)

Quarter-wave drift tube structures exhibit rf magnetic fields on the beam axis which steer the beam and can cause significant emittance growth. A method of shaping the drift-tube to substantially reduce steering has been developed and will be tested in the prototype 115 MHz QWR cavity.

a.4. **Superconducting RF: Upgraded Surface Processing and Single-Spoke Cavity Performance** (K. W. Shepard, Joel Fuerst, Michael Kelly, and Mark Kedzie)

Figure III-5 shows the computer-controlled, automated high-pressure water rinse apparatus for cleaning and removing particulate contaminants from high-field niobium drift-tube cavities. The upgraded facility was used to process a β=0.4 350 MHz niobium spoke cavity and obtain an accelerating gradient of 7 MV/m at T = 4.3 K and 10 W of input rf power as shown in Fig. III-6. The cavity was subsequently operated cw 24 hours/day for 28 days at 7 MV/m with no performance degradation, evidence that properly cleaned drift-tube cavities can operate at high fields for extended periods of time in a realistic accelerator environment.

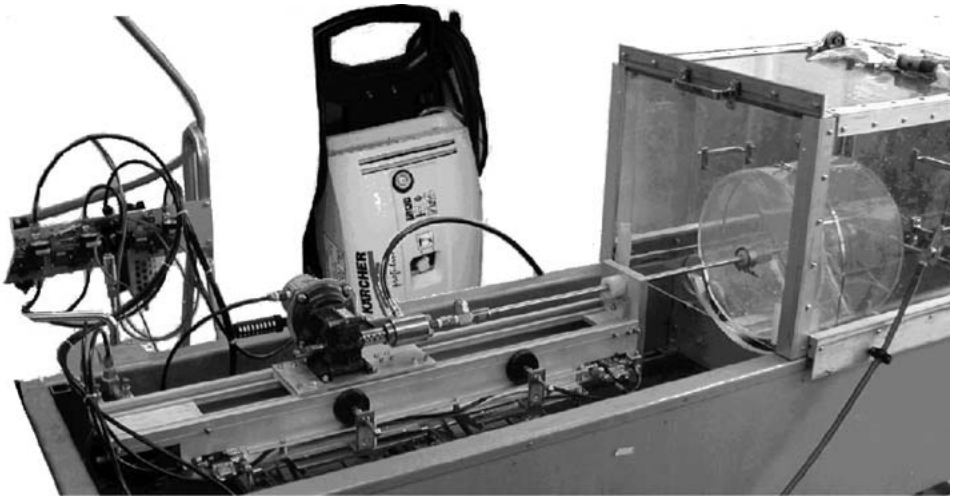

Fig. III-5. Automated, computer-controlled high-pressure water rinse apparatus.

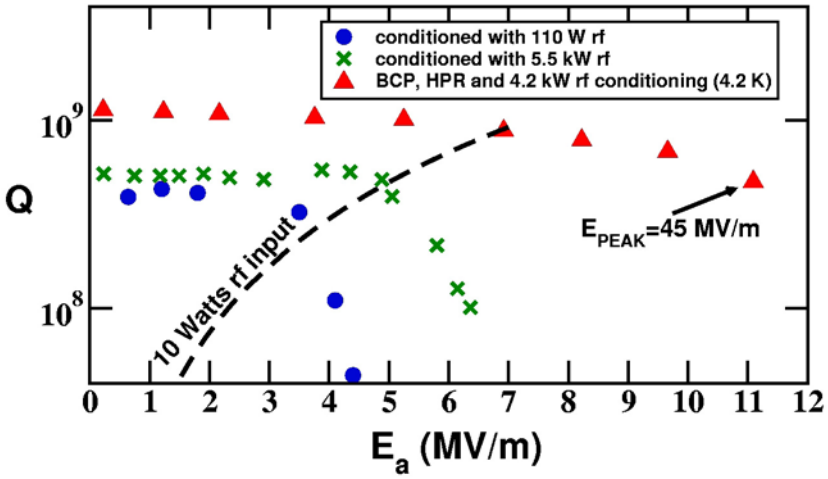

Fig. III-6. Performance of a 350 MHz single-cell spoke cavity after buffered chemical polish (BCP) and high-pressure water rinse using the upgraded facility.

a.5. RIA Cryogenics (J. R. Specht)

Major efforts this year were devoted to issues related to the liquid helium refrigerator, its loads and systems, and a distribution system. The cryogenic plant would be two times the size of the TJLab/CEBAF system and because of the variable load requirements, with an assortment of 2.0 K, 4.4 K, 35 K, and liquefaction loads, will require a complex and reliable cryogenic plant and distribution system.

Two separate vacuum insulated coaxial lines, a supply and return, will be used along all portions of the system. There are four types of lines used at RIA. These are tabulated below. All four types are similar in design, only the dimensions of the various parts change. Exact dimensions have yet to be determined for all the lines listed. Preliminary pressure drop calculations have been made using the mass flow for each line and the dimensions of the TJNAF/CEBAF lines. Some of the lines will need to be made larger because of their length and the additional mass flow. Vacuum breaks will be installed at regular intervals along all of the distribution lines. This will provide isolation and allow for leak detection. The linac supply and return lines have the required bayonet ports, valves, and expansion/contraction built in at the appropriate spacing to match the various cryostat lengths. The LN2 distribution will use sub-cooled liquid to allow single phase liquid to be delivered to the various loads. The 2.0 K linac and 4.4 K linac return lines differ in the type and size u-tubes/bayonet used. Vacuum guarding is used in the 2.0 K sub-atmospheric returns along with larger u-tubes. The distribution system will accommodate cool-down, normal operation, and maintenance modes. Removable u-tubes will permit removal of cryostats for maintenance activities.

Line Type	Portion of coaxial line	Supply Line	Return Line	Length (m)
4 K linac	inner	4.4 K @ 3 bar He	4.4 K @ 1.5 bar He	259
	outer	80 K @ 3 bar LN_2	80 K @ 1.5 bar N_2	259
4 K CHR	inner	4.4 K @ 3 bar He	4.4 K @ 1.5 bar He	350
	outer	80 K @ 3 bar LN_2	80 K @ 1.5 bar N_2	350
2 K linac	inner	4.4 K @ 3 bar He	3.5 K @ 0.03bar He	316
	outer	35 K @ 5 bar He	50 K @ 5 bar He	316
2 K CHR	inner	4.4 K @ 3 bar He	3.5 K @ 0.03 bar He	28
	outer	35 K @ 5 bar He	50 K @ 5 bar He	28

The Central Helium Refrigerator (CHR) must be able to operate efficiently with different loads. Because the driver and post linac's ion and energy are variable, different loads will be presented to the refrigerator for various accelerator requirements. In order to reduce the operating expenses, turndown capability will be required.

PLANT REQUIREMENTS	TEMPERATURE (K)	PRESSURE at LOAD (bar)	DESIGN	OFF-DESIGN
REFRIGERATION	4.6	1.50	5.0 kW	1.80 kW
REFRIGERATION	2.0	0.03	8.6 kW	0.60 kW
LIQUEFACTION	4.6	1.50	15 g/s	15 g/s
SHIELD COOLING	35	5	15.3 g/s	15.3 g/s

Tabulated here are the requirements for the refrigerator. Because of its large size, the cold box would be built in several sections. Cold box #1 would be an 80 K system while cold box #2 would contain the 4 K system. The cold compressors will be located in cold box #3. This allows the 4.4 K portion of the cryogenic system to maintain liquid helium in the linacs if maintenance is required on the cold compressors. A system block diagram is shown in Fig. III-7. The cycle used for the refrigerator has yet to be chosen. There are

two major types to be considered to provide the sub-atmospheric 2.0 K portion: 1) cold-compressors only or 2) cold compressors along with room temperature compressors. Each of these methods has original hardware investment costs with an associated operating cost as well as operating advantages/disadvantages. An optimization of cost versus benefits will be necessary to determine which cycle is best suited to this project.

The total inventory of LHe in the RIA system is about 73,000 L. A 20,000 gallon dewar would provide an adequate storage capacity for the liquid, while eight 30,000 gallon warm storage tanks would provide a reasonable buffer for the gas management system.

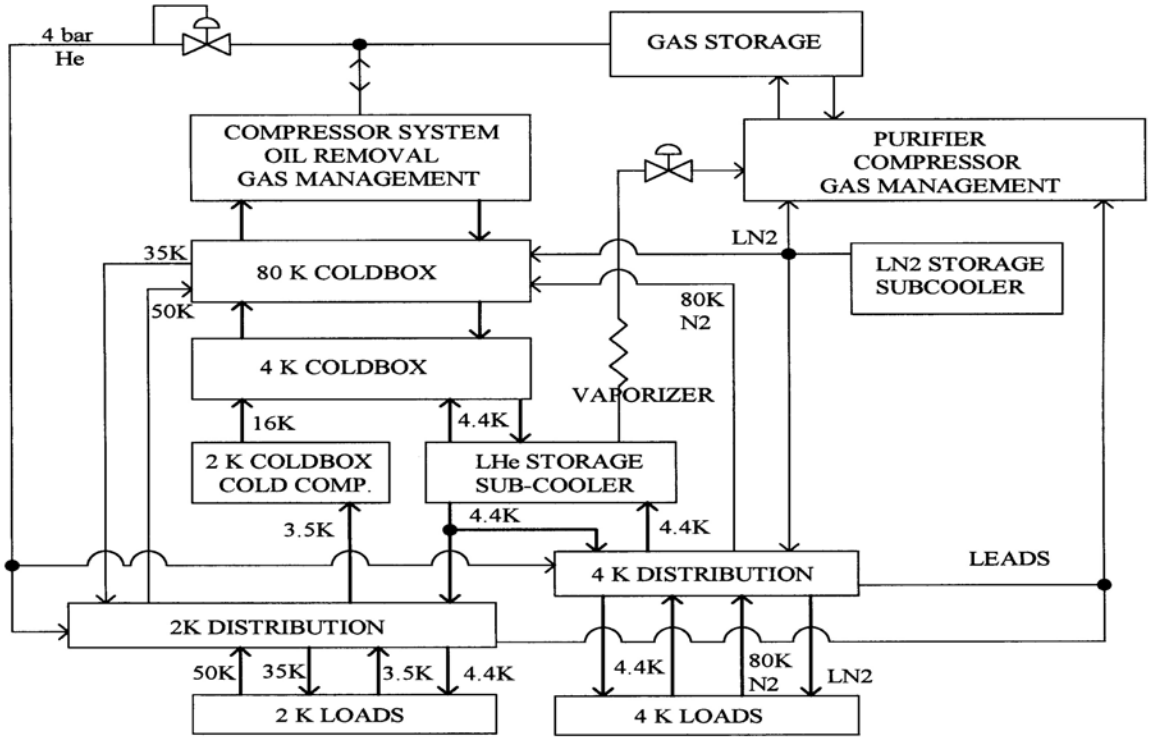

Fig. III-7. A block diagram of the RIA cryogenics system.

High reliability is a must for the RIA cryogenic plant. Because of the large capital cost for large refrigerators, a redundant or stand-by refrigerator may not be included in the initial construction. To improve the reliability of the refrigeration system, several additional pieces of hardware will be required: 1) a reliable and flexible control system, 2) a warm gas purification system, and 3) a gas recovery system.

a.6. **Development of a Superconducting Solenoid for the RIA Facility** (P.N. Ostroumov, K.W. Shepard, and S.H. Kim*)

The beam dynamics of the drift tube section of the driver linac require a compact accelerating-focusing lattice. The use of SC solenoids together with SRF resonators within a common cryostat can solve this problem. The solenoids must have low fringing fields to avoid magnetic flux capture in the SRF resonators. Also, the compactness of the linac lattice can be increased by incorporating dipole steering coils together with the SC solenoids in one magnet assembly. R&D work has been carried out to determine the feasibility of combining the three elements of high solenoid field, low fringe field, and integral dipole field into one compact package. A 9 Tesla magnet has been initially designed and prototyped, with the goal of eventually developing 14 Tesla solenoids of similar design. The most important design issues are 1) to minimize stray field in the RF cavity region using superconducting bucking coils and 2) to achieve adequate mechanical

*AOD Division, Argonne National Laboratory.

stability of the transverse dipole windings in the presence of forces produced by the solenoid/bucking coil assembly. The overall length of the prototype magnet assembly is 30 cm and includes a 9 Tesla solenoid formed from 4 coaxial sections, 2 coaxial bucking coils along the Z axis at each end of the solenoid, and a steering dipole producing 0.2 Tesla on the Y axis. An exploded view of the magnet assembly is shown in Fig. III-8. The bucking coils produce a low-field region, less than 0.1 Tesla, between 15 and 18 cm from the magnet center. Axial profile of the solenoidal magnetic field is shown in Fig. III-9. The racetrack coil is a constant current winding and located at 45 degree with respect to X and Y axes. Dipole field distribution from the coil is uniform. Within 10-mm circle dB/B is less than 1% and within 12-mm less than 1.5%. The dipole field distribution in the XY plane is shown in Fig. III-10.

The assembly including terminals, switches and protection circuit are designed to fit inside a 25 cm diameter helium reservoir. The magnet assembly will be constructed in cooperation with TRIUMF (Vancouver, Canada) and tested at ANL.

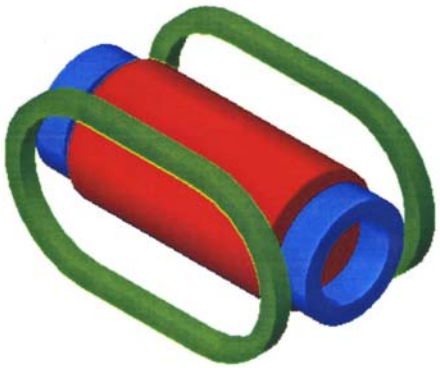

Fig. III-8. An exploded view of the superconducting magnet assembly containing solenoid, bucking coils and racetrack coils.

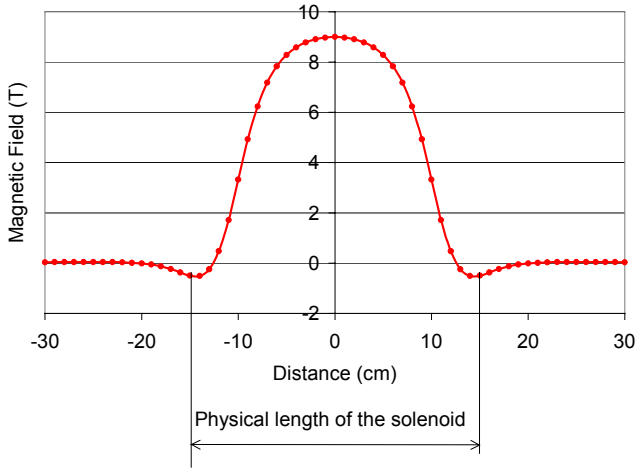

Fig. III-9. Profile of the magnetic field on the solenoid axis.

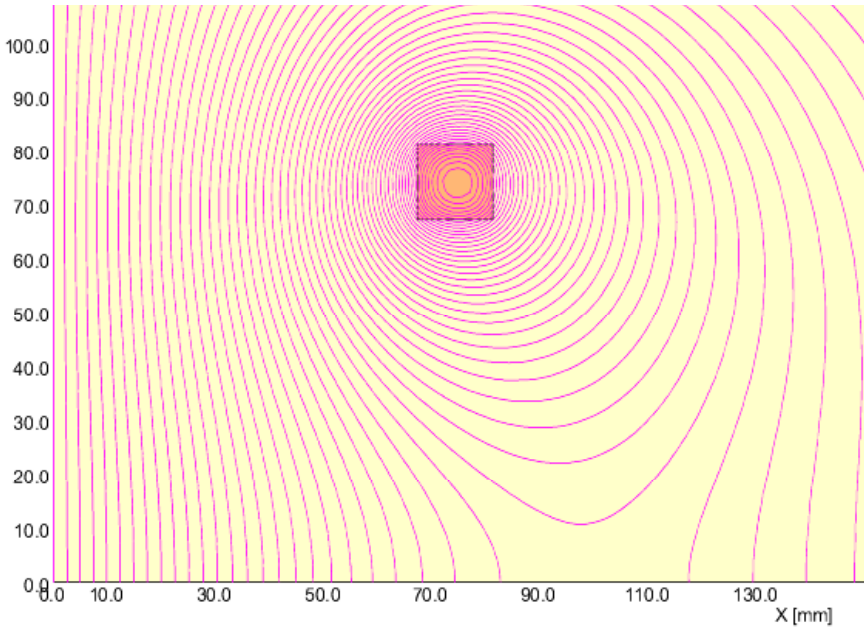

Fig. III-10. The magnetic flux lines of the racetrack coil are shown in the first quadrant. The coil-winding cross section is 14 × 14 with its center at (x,y) = (74,74) in mm units. The magnetic field at the origin is 0.2 T @ 31.7 kA. The field uniformity within 10 mm from the origin is better than 1%

a.7. **57.5 MHz CW RFQ for the Driver Linac** (P.N. Ostroumov and A.A. Kolomiets)

In the driver linac the initial acceleration of heavy-ions delivered from an ECR ion source can be effectively performed by a 57.5 MHz four-meter long room temperature RFQ. The principal specifications of the RFQ are: 1) formation of extremely low longitudinal emittance; 2) stable operation over a wide range of voltage for acceleration of various ion species needed for RIA operation; 3) simultaneous acceleration of two-charge states of uranium ions. CW operation of an accelerating structure leads to a number of requirements for the resonators such as high shunt impedance, efficient water cooling of all parts of the resonant cavity, mechanical stability together with precise alignment, reliable rf contacts, a stable operating mode and fine tuning of the resonant frequency during operation. To satisfy these requirements a new resonant structure has been developed. This new RFQ structure provides 57.5 MHz resonant frequency within a tank of 0.56 meter diameter. Three-dimensional electromagnetic, thermal, and structural analysis of the structure have been completed, and a mechanical design based on a brazing technique is being developed. Figure III-11 shows 57.5 MHz RFQ resonant structure and engineering design of one section. The full RFQ will contain 6 such sections (see Fig. III-12).

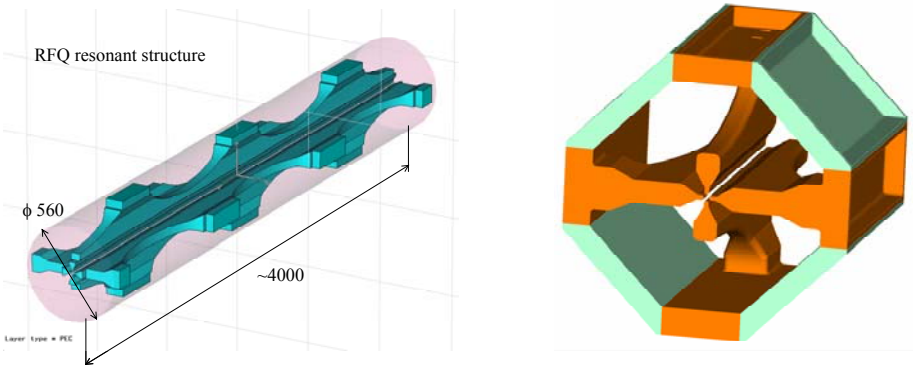

Fig. III-11. 57.5 MHz CW RFQ. On the left: computer model for electrodynamics simulations; On the right: engineering computer model of a RFQ section.

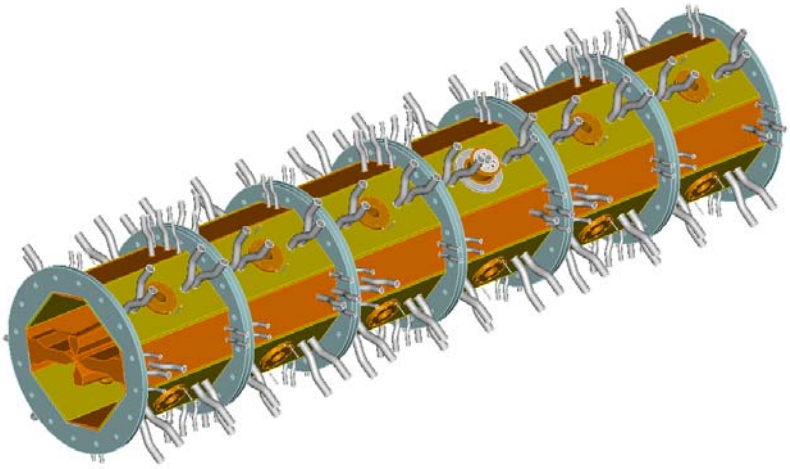

Figure III-12. Computer model of the RFQ final assembly, 6 sections.

a.8. 12.125 MHz Accelerating Structure: The Hybrid RFQ (P.N. Ostroumov, A.A. Kolomiets, J.A. Nolen, S. Sharma,* E. Rotela,* A. Barcikowski†)

Several resonant structures have been considered as candidates for the hybrid RFQ. The main specifications for our application are: 1) the structure length ~3.34 m is determined by the given input and output beam energies; 2) the structure should be mechanically stable; and 3) the shunt impedance should be high. Though split-coaxial structures have been used in several low frequency RFQs, the Wideroe-type structure better satisfies the abovementioned conditions. The side view of the accelerating structure used for the electrodynamics simulation by the code Microwave Studio (MWS) is shown in Fig. III-13. An engineering model of the first section of the H-RFQ containing 13 drift tubes is shown in Fig. III-14. According to MWS the rf losses are 11.6 kW at 100 kV inter-vane voltage in this copper resonator. The losses are lower than in split-coaxial RFQ of similar length because the total capacitive loading of the drift tubes is about half that of the four-vane structure. Due to the short length of the structure compared to the wavelength, a voltage distribution on all vanes and drift tubes is uniform which is confirmed by 3D simulations. For verification of electrodynamics properties of the H-RFQ we decided to build a half-scale cold model. Figure III-15 shows general side view of the model during the assembly. Detailed study of the model with the goal of determination of final resonator dimensions, accelerating and focusing field distribution and coupling to the external power supply will be carried out in the near future.

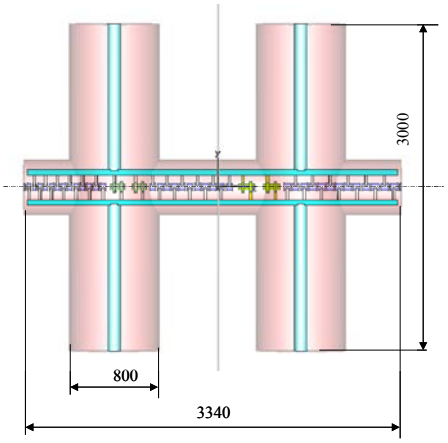

Fig. III-13. Side view of the hybrid RFQ accelerating structure. (Dimensions are in mm.)

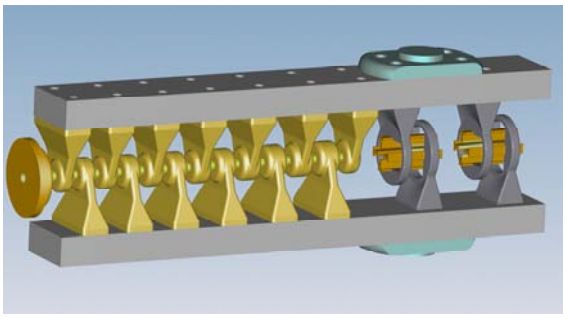

Fig. III-14. Computer drawing of the first section of the accelerating structure.

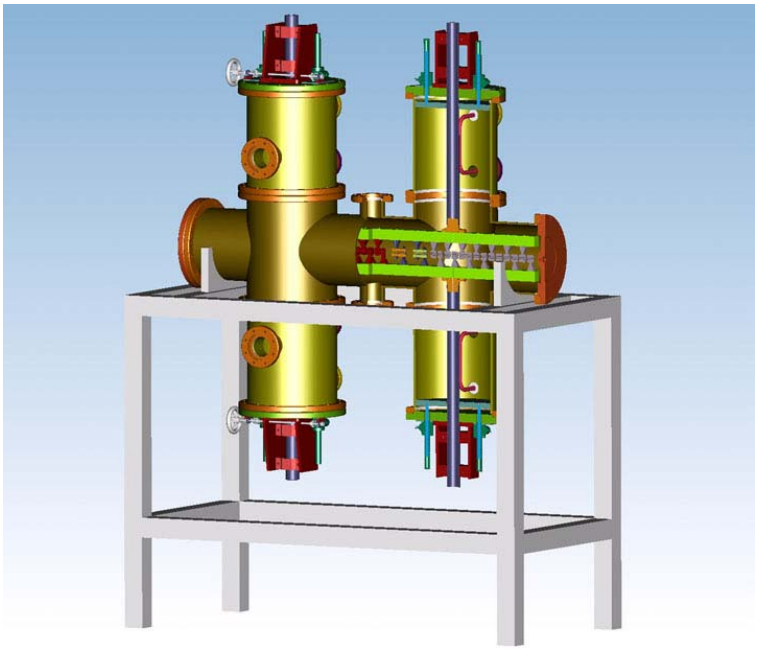

Fig. III-15. Computer drawing of the 12 MHz Hybrid RFQ half-scale cold model.

*AOD Division, Argonne National Laboratory.
†ASD Division, Argonne National Laboratory.

B. RIA BEAM DYNAMICS

b.1. Update of the Driver Linac Benchmark Design (P.N. Ostroumov, K.W. Shepard)

Significant progress has been made in beam dynamics design of the RIA driver linac. This linac will accelerate multiple-charge-states (multi-q) of the heaviest ion beams, for which the beam current is limited by ion-source performance. Beam dynamics studies have been performed with the goal of optimization of the linac structure in order to reduce a possible effective emittance growth of multi-q uranium beam. The location of two strippers naturally divides the linac into the three parts: low-, medium-, and high-beta sections. A detailed design has been developed for the focusing-accelerating lattice of the linac. The sources of the effective emittance growth have been identified. In longitudinal phase space main sources of the emittance growth are 1) multiplicity of charge states; 2) random errors of rf field; 3) passage of the stripper and 4) effect of higher-order terms in the field expansion in the multi-q beam transport systems. In the transverse phase space similar sources are 1) misalignments of SC resonators and focusing elements and their effect on multi-q beam emittance; 2) passage of the stripper and 3) effect of higher-order terms in the field expansion in the multi-q beam transport systems.

Long inter-cryostat spaces in the low- and medium-β sections will require the large stability area in the longitudinal phase space which can result in cavity setting at high value of synchronous phases. Therefore several important measures will be applied in order to minimize the length of the inter-cryostat spaces and to facilitate an impact of the drift spaces on the beam dynamics:

- The RFQ and multi-harmonic buncher are specially designed in order to provide very low longitudinal emittance of two charge-state uranium beam.
- Inter-cryostat space will contain only vacuum valves and a beam profile monitor. These devices will be designed for the lowest possible space occupation along the beamline.
- Beam steering coils will be combined with the SC focusing solenoids and will not require an additional space along the beamline.
- Standard accelerating SRF cavities can be switched to the mode of a beam phase monitor in order to set up phases and amplitudes of the accelerating fields in the upstream cavities. No space is required for beam phase monitors between the cryostats.
- Transverse matching between the cryostats is facilitated by the absence of the first SRF cavity in the very first focusing period of the cryostats. This focusing period incorporates inter-cryostat drift space instead of the SRF cavity.
- A special transition section is designed between the first two cryostats of low-β linac where beam energy is low and beam matching is extremely critical to the length of the drift space.

The effective longitudinal emittance of multi-q uranium beam oscillates along the linac sections as is shown in Fig. III-16 due to the slightly different synchronous phases of each charge state. The beam energy exiting low- and medium-beta sections should be selected in order to obtain the lowest effective emittance for the multi-q uranium beam.

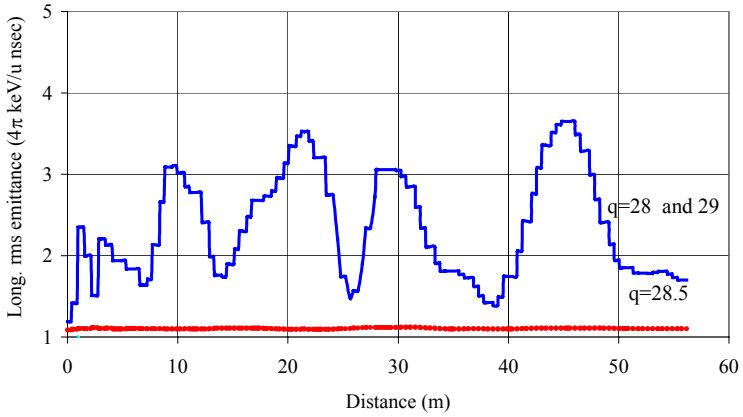

Fig. III-16. RMS longitudinal emittance variation of single- (the red curve) and two charge-state (the blue curve) beams along the low-β linac.

To insure all requirements can be met, we have numerically simulated the dynamics of multi-q uranium beams from the ion source, through the driver linac, all the way to the production targets. These simulations have been iterated repeatedly with the design for the overall linac architecture.

The code TRACK has been written in order to integrate charged particle motion in the presence of all components of the electromagnetic field. The electromagnetic fields in all types of SRF cavities were obtained from the code CST Microwave Studio (MWS). The TRACK code simulates multi-particle motion in six-dimensional phase space by an iterative solution of the equations of motion. The MWS code running on modern PCs can calculate all six components of electromagnetic field distributions within the beam-cavity interaction area with a mesh size less than 1 mm. The simulation of beam dynamics in the presence of all components of both electric and magnetic fields is essential in superconducting quarter-wave resonators (SC QWR). The driver linac will use more than 85 QWRs operating at 57.5 MHz and 115 MHz.

Beam dynamics simulation in each of the three sections of the driver linac included the following steps:

- Beam matching in transverse and longitudinal phase spaces for a trial beam with the mean value of charge-to-mass ratio. Simulation of the trial ion beam to minimize beam sizes, to obtain smooth rms envelopes in transverse planes. The rms oscillations in longitudinal phase space due to the effect of inter-cavity drift spaces were minimized but not eliminated completely. In the parts of the linac the synchronous phase is equal to –30°, which produces a large linear region for the beam size oscillations. Therefore the longitudinal emittance of the trial beam does not grow.
- Simulation of a multi-q beam. Final determination of beam energies at stripping foil and total required number of the cavities.
- Beam dynamics simulation of the multi-q beam under the effect of random errors both in transverse and longitudinal phase space.

The simulations, which include misalignments of focusing and accelerating elements and random errors of the rf fields, show that beam emittances are well within the six-dimensional acceptance of the driver linac. The results of this simulation are summarized in Fig. III-17. The latter shows longitudinal phase space plot of 400 MeV/u multi-q uranium beam including all errors of rf field and amplitude along the whole linac. As is seen the multi-q uranium beam can be accelerated up to 400 MeV/u within ±0.25% of energy spread and remains within ±10° phase width. The longitudinal effective emittance 75.8 π·keV/u·nsec contains all particles shown in Fig. III-17.

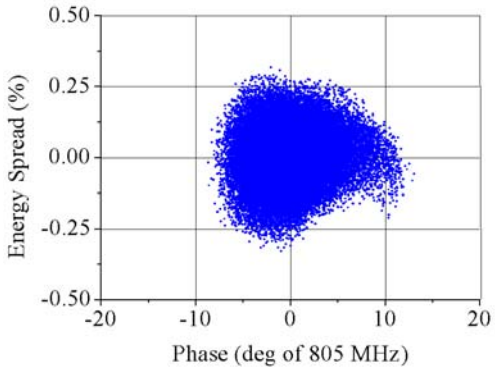

Fig. III-17. Longitudinal phase space plots of a four charge state uranium beam at the exit of the driver linac.

b.2. Low-Charge State Heavy-Ion Beam Dynamics in the Hybrid RFQ (P.N. Ostroumov, A.A. Kolomiets, N.E. Vinogradov)

A design has been developed for a low charge state injector for the RIB linac to provide for the post-acceleration of singly-charged beams as heavy as uranium. A RIB linac will accelerate heavy ions in the mass range 6 to 240, initially with charge state 1+. The acceleration of slow, low-charge-state heavy ion beams is a difficult problem. A device that can be utilized is a conventional RFQ accelerator. The rf electric fields of such devices are very effective at focusing heavy ions, but the longitudinal electric field provided only by the vane modulations makes it an inefficient accelerating structure. For low velocity ions the structure must

operate at a low rf frequency leading to a very large and expensive structure. To overcome this drawback we proposed a hybrid accelerating structure that is formed by an alternating series of drift tubes (DTL) and RFQ sections. In such a structure the accelerating and focusing functions are decoupled. An unmodulated four-vane RFQ forms two sections each with length $\beta\lambda$ separated by a drift space $\beta\lambda/2$. The focusing strength of each RFQ lens with the length $\beta\lambda/2$ is adjusted and fixed by the aperture radius R_0. A section of the RFQ with length $\beta\lambda$ acts as a "doublet". The drift space between the "doublet" is necessary in order to ease the required electric field between the vanes. The whole focusing system works as a symmetric triplet. At higher q/m lower focusing gradients are required and it can be shown that in such cases the RFQ triplet can contain only three $\beta\lambda/2$ cells. A remarkable feature of the RFQ triplet is the lack of fringing field effects because the arrival time of beam bunches is synchronized to zero field at the edges of the RFQ vanes.

A hybrid RFQ (H-RFQ) operating at 12 MHz was designed for acceleration of heavy ion beams with q/A=1/240. The accelerating structure is ~3.4 m long and consists of three sections of DTL and two sections of RFQ. Each section of the DTL comprises 10 to 14 drift tubes. The RFQ sections comprise five $\beta\lambda/2$ cells and form a focusing triplet. The average accelerating gradient of the H-RFQ is about twice that of a conventional RFQ while the transverse acceptances are the same for both types of accelerator. Figure III-18 shows the accelerating efficiency of the hybrid RFQ compared to the conventional RFQ.

We have designed a cw H-RFQ for acceleration of singly-charged uranium in the front end of the RIB linac. For cw operation the peak surface field must be chosen very carefully. Our design is based on a 12 MHz accelerating structure with 100 kV between the drift tubes (DT) and RFQ vanes. The peak surface electric field occurs on the vanes of the first RFQ lens and it is 20% lower than in our previously tested 12-MHz split-coaxial RFQ structure. The surface field on the drift tubes is kept even lower by selecting long accelerating gaps.

The results of three-dimensional beam dynamics simulations in the H-RFQ performed with the DYNAMION code are shown in Fig. III-19. In these simulations 2D electric fields in the accelerating gaps are calculated with DYNAMION and 3D fields in the RFQs calculated with the SIMION code.

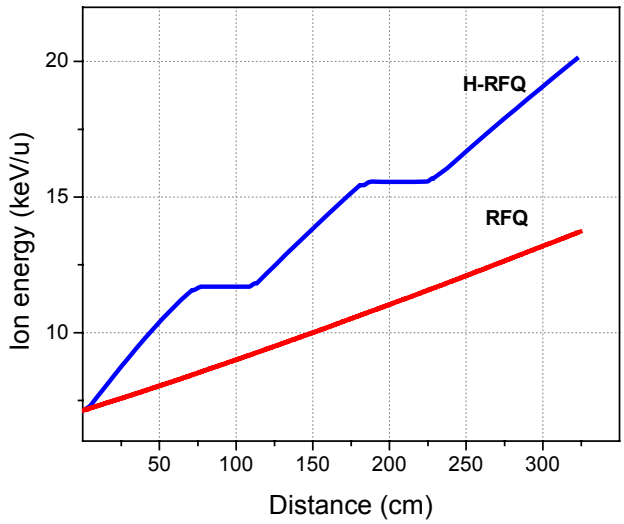

Fig. III-18. Beam energy gain in the hybrid and conventional RFQs. The structures have equal voltage between electrodes.

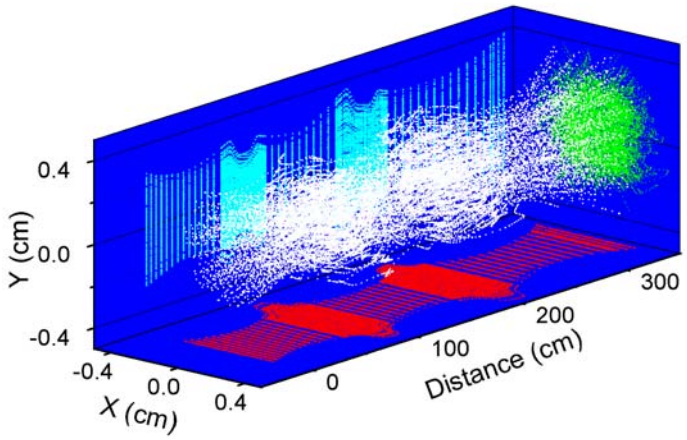

Fig. III-19. Particle trajectories along the H-RFQ shown in real space.

b.3. **Correction of Beam Steering Effects in Low-Velocity Superconducting Quarter-Wave Cavities** (P.N. Ostroumov and K.W. Shepard)

Superconducting cavities presently used for acceleration of ions in velocity range ~0.01c to 0.3c are based on quarter-wave resonators (QWR). Currently there are several design proposals in nuclear physics laboratories for application of this type of cavity for acceleration of light and heavy ions. Particularly, the RIA project will use about 85 QWRs. The operating frequencies of the cavities range from ~50 MHZ to 360 MHz to satisfy various specifications. Electrodynamics studies of the field distributions in the beam-cavity interaction area indicate appreciable steering components of both electric and magnetic fields, especially for higher-frequency cavities. The dipole fields induce beam steering, which is a strong function of rf phase and which couples the longitudinal and transverse motions. This can result in growth in the transverse emittance of the beam. Such steering effects are most pronounced for light ions. While simple steering, or displacement of the beam centroid, can be compensated by using standard, static corrective steering elements, the present case is complicated by the phase dependence of both the electric and magnetic fields. In a two-gap QWR the phase-dependence of steering for both the electric dipole field and the magnetic field is shifted 90 degrees from the accelerating field. This means that at typical operating RF phase angles, the steering is a strong function of RF phase and couples the longitudinal and transverse motion. As a result, the steering fields can, depending on the longitudinal emittance, induce appreciable transverse emittance growth. Such emittance growth can not be compensated by static fields and can be a particularly serious problem in applications for high-intensity light-ion beams.

We found that the steering can be largely compensated by two different methods. Simply offsetting the cavities by a few mm can often provide adequate compensation. In this method, available range of steering is limited by the reduction of useful aperture of the linac. This method does not require manufacture of new types of cavities and can be applied for heavy-ion accelerators dealing with $q/A<1/3$ in the velocity range ~0.01c-0.15c. More generally, steering can be largely eliminated over the entire useful velocity range by shaping the drift-tube and cavity-wall faces adjacent to the beam axis to provide appropriate corrective vertical electric field components.

The particular examples of two quarter-wave resonators operating at 57.5 and 115 MHz designed for the driver linac of the Rare Isotope Accelerator (RIA) facility were analyzed. We have numerically modeled the electrodynamic properties and field distributions using Microwave Studio (MWS). The distributions of E_z, E_y and H_x on the axis of the 115 MHz QWR are shown in Fig. III-20. As is seen there is an appreciable magnetic field, ~60 G in the accelerating gaps. The TRACK code was used to simulate a section of the RIA driver linac containing forty-two 115 MHz cavities. Multi-particle simulation of uranium and proton beams was carried out in the linac with modified, steering-corrected QWRs. The results of proton beam simulations are shown in Fig. III-21. As is seen transverse emittance growth is almost completely eliminated.

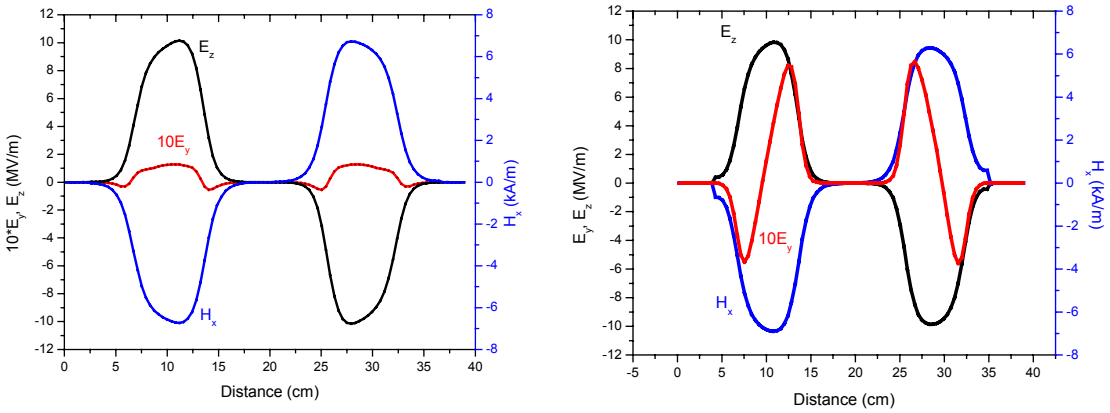

Fig. III-20. Field distribution along the axis of the 115 MHz QWR before (the left) and after (the right) the modifications to correct beam steering. For the clarity magnetic field is shown with opposite sign with respect to the electric field. The amplitude of E_y is multiplied by a factor of 10.

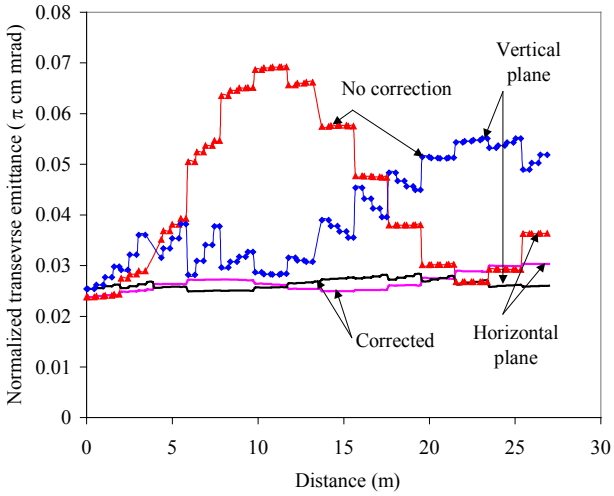

Fig. III-21. Transverse emittance growth in the section of driver linac containing 42 cavities of 115 MHz QWR with and without the compensation of beam steering effect.

b.4. Design of the RIA Driver Linac Switchyard (J.A. Nolen, V.N. Aseev, P. N. Ostroumov, and S. Kim*)

We have completed a preliminary design for a driver linac switchyard which can deliver beams to four production targets. Driver beam power of up to 400 kW will be available so that beam sharing between target stations is desirable. Design of the switchyard for the driver beams of RIA is a unique task due to the following features: 1) Distribution of various ion species accelerated to a wide range of energies to four target stations; 2) Delivery of beams to two target stations simultaneously; 3) Providing high quality beam optics with higher order corrections for multiple charge state beams to produce small beam spots at the entrance of the fragment separators. A rf sweeper is used for beam delivery to two targets simultaneously. The rf-sweeper is followed by two DC septum magnets. A room temperature IH-type cavity operating at 115 MHz is proposed for the rf-sweeper and it provides four-milliradian beam deflection. Figure III-22 shows layout of the beam switchyard. Beam envelopes of a four-charge state uranium beam in the transport system from the linac exit to the fragmentation targets are shown in Fig. III-23. The multi-q uranium beam can be focused to a spot $X \times Y = 1.0 \times 3.0$ mm^2.

*AOD Division, Argonne National Laboratory.

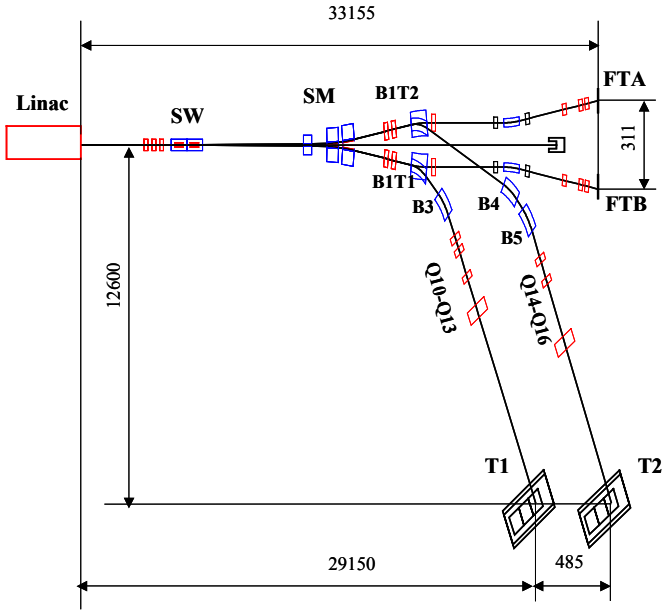

Fig. III-22. Layout of the driver linac switchyard. The distances are shown in mm. Legend: SW – rf sweeper; SM – septum magnets; B1T1, B1T2, B3, B4, B5 – bending magnets; Q10-Q13,Q14-Q16 – quadrupoles; FTA, FTB – fragmentation targets; T1, T2 – ISOL targets.

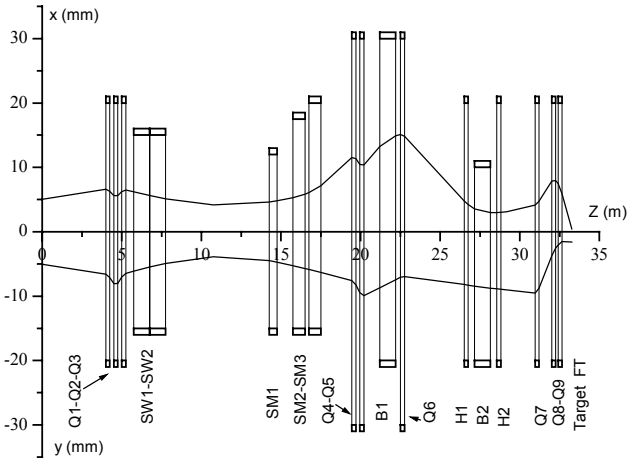

Fig.III-23. Multi-q uranium beam envelopes along the beamline from the linac to fragment separator targets FTA and FTB.

C. RARE ISOTOPE PRODUCTION, SEPARATION, AND DIAGNOSTICS

c.1. **Bunch Shape Monitor for CW Heavy-Ion Beams** (P.N. Ostroumov, P. Billquist, R.C. Pardo, M. Portillo, S. Sharamentov, N.E. Vinogradov, and G.P. Zinkann)

A new device for the measurement of CW heavy-ion beam time profiles with ~20 picosecond resolution has been constructed and successfully commissioned at ATLAS. Figure III-24 shows the general view of the BSM located ~3 m downstream of the Booster. The Bunch Shape Monitor (BSM) is based on the analysis of secondary electrons produced by a primary beam hitting a tungsten wire to which a potential of -10 kV is applied. In a BSM the longitudinal distribution of charge of the primary beam is coherently transformed into a spatial distribution of low energy secondary electrons through transverse rf modulation. This modulation is provided by a 97 MHz rf sweeper. The distribution of secondary electrons is detected by a chevron MCP coupled to a phosphor screen. The signal image on the screen is measured by using a CCD camera connected to the PC. Several test measurements have been done. First, a prebunched low energy (30 MeV) oxygen beam from tandem was transported to the BSM location. The FWHM of the bunch width was measured at the level of 2 nanoseconds. Recent measurements were done for an 80 MeV neon beam accelerated in the Booster. Typical beam currents in these measurements was from several pnA to 100 pnA. The longitudinal profile of the 80 MeV neon beam is shown in Fig. III-25. The resolution of the BSM depends from rf power in the sweeper. For this particular measurement the resolution was 30 picoseconds and the pulse width is 260 psec as shown. At this moment the time resolution is restricted by the background noise. It seems that this noise is caused by low energy secondary electrons produced by ions on beamline components and the residual gas. Additional measures to eliminate the background noise are being studied.

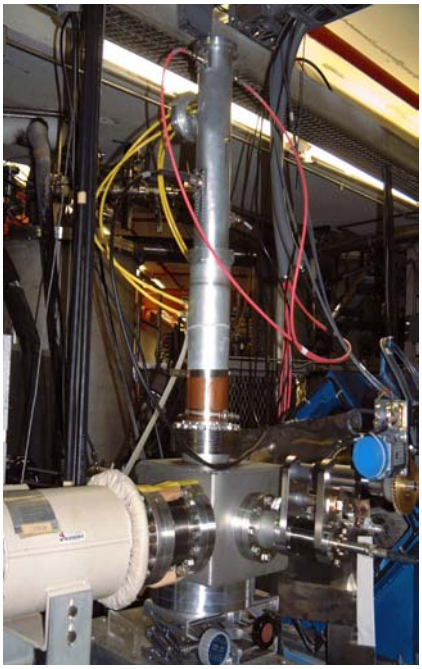

Fig. III-24. Bunch Shape Monitor installed at the exit of the Booster.

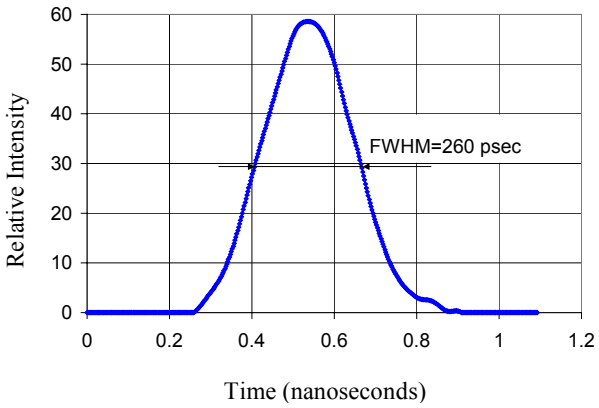

Fig. III-25. Longitudinal profile of 80 MeV $^{20}Ne^{8+}$ (the background noise is subtracted).

c.2. **Assessment of the Radioactive Inventory Produced by the Current RIA Target Designs** (I.C. Gomes and J.A. Nolen)

The Rare Isotope Accelerator (RIA) will produce besides the isotopes of interest by-products that will constitute a radioactive inventory in the facility. The large majority of these by-products will be produced in the target material during beam bombardment. The assessment of the radioactive inventory is important to classify the facility based on the Hazard Class Limits from DOE-STD-1027-92. During the assessment of the radioactive inventory a few assumptions were made, such as:

a) All by-products produced during irradiation would stay in the target for the full length of the irradiation;
b) That the target configuration is feasible meaning that the amount of target material would be compatible with a real target configuration;
c) That there is no accumulation of inventory meaning that all radioactivity produced is carried to an outside repository when the irradiation ends; and
d) That other materials inside the target cell would have negligible contribution to the radioactivity inventory.

The analysis was carried out for two-step, direct, and fragmentation targets. The two-step target was composed of a primary 9-cm long, 1-cm diameter tungsten target and a secondary hollow cylinder 15-cm long with 2-cm internal diameter and 11-cm external diameter 2.5g/cm^3 UC target. The direct target was 5g/cm^2 UC target with a large copper beam-stop. Both the direct and two-step target were bombarded by 1.2-GeV deuteron beam. The fragmentation estimate was selected by considering the worst combination of a heavy ion beam with a lithium target. It was found that the two-step target produces the highest radioactive inventory among the configurations studied. Also, it was found that the fission product ^{131}I is the most offending isotope relative to the regulations. The calculations have shown that RIA is most likely to be classified as a Class 3 nuclear facility for the target cells and an accelerator facility otherwise.

Figure III-26 shows the ratio of the radioactive isotope accumulated for the two-step target during irradiation to the Class-3 inventory limit based on the DOE-STD-1027-92. It can be noticed that a large number of radioactive products are generated, however, just a few are produced in significant quantity. Table 1 shows the ratio to the Category-3 and Category-2 limits of those isotopes from the direct-target configuration with the largest ratios. Table 2 presents the same data as Table 1 for the two-step target. None of the isotopes is expected to have an inventory greater than the Category-2 limit.

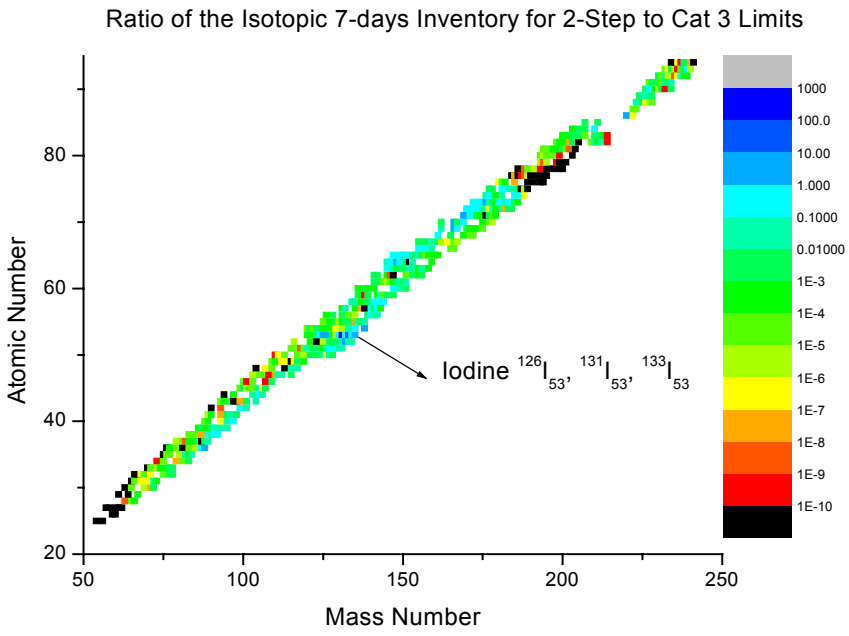

Fig. III-26. Ratio of the isotopic inventory accumulated after 7 (seven) days of continuous operation of a two-step target in RIA (1.2-GeV deuteron beam on tungsten with UC-2.5g/cm^3 as secondary target) to the DOE Category-3 inventory limit.

Table 1. Ratio (of the products that have surpassed Category-3 limits) to the Category-2 and Category-3 limits. Isotopes indicated as "N/A" have no limit set by the DOE for Category 2 for that isotope, however all of them are barely over Category 3 limits and they should not be of any concern.

Isotope	**Cat-2**	**Cat-3**	Isotope	**Cat-2**	**Cat-3**
P-32	4.341e-03	1.602	**I-125**	3.152e-04	1.351
Mn-52	4.594e-04	5.404	**I-126**	N/A	3.423
Co-56	N/A	1.601	**I-131**	9.036e-03	17.68
Co-58	N/A	1.389	**I-133**	N/A	2.167
Cu-61	N/A	2.251	**Po-210**	2.435e-03	0.449
Cu-64	N/A	9.497	**Rn-220**	N/A	1.464

Table 2. Ratio of the isotopes that have concentration above Category-3 limit to the Category-2 limits for the Two-Step Configuration.

Isotope	**Cat-2**	**Cat-3**	Isotope	**Cat-2**	**Cat-3**	Isotope	**Cat-2**	**Cat-3**
Kr-88	N/A	1.038	**I-126**	N/A	4.185	**I-135**	N/A	2.537
Te-132	N/A	1.088	**I-131**	0.162	316.3	**Tm-166**	N/A	2.488
I-125	0.00029	1.234	**I-133**	N/A	55.2	**Ta-176**	N/A	2.297

c.3. Implementation of Computer Codes for Use in the RIA Target Design Activities at the NERSC (I. C. Gomes and J. A. Nolen)

The National Energy Research Super-Computer Center (NERSC) is a computer center supported by the DOE for the research community. NERSC currently has the most powerful non-classified and third most powerful computer on Earth, a 3,328-processor IBM supercomputer. The use of the computers at NERSC for RIA design activities has been on a trial basis because of the highly parallel computer environment structure used at NERSC. Computer codes such as MCNP, CINDER and TRAC (Transient Reactor Analysis Code) were successfully implemented at NERSC but only MCNP was used for production calculations in parallel mode. In the future it is expected to have MCNPX running in parallel mode at NERSC to take advantage of the savings in turnaround time that parallel processing can provide. Monte Carlo computer codes are highly suitable for parallel processing because of the intrinsic independence between histories. Parallel processing allows several Monte Carlo random walks to be performed at different processors and the relevant information stored in a common tally array. The RIA activities have received good support from NERSC through availability of computer time and some technical support but there is not yet a heavy use of these computers because of the need for NERSC compatible parallel versions of the codes. Efforts have been devoted to obtain parallel versions of the codes but unfortunately, the operational system used at NERSC is not considered a high priority among code developers at the present time. However, it is expected that with modest support some codes can be implemented at NERC, such as the MCNPX and others.

Currently there is a continuous effort to implement codes and data libraries that can support RIA target design activities. Due to the nature of RIA it will be necessary to adapt several codes to produce necessary engineering design parameters for target assessment. Quantities such as rare isotope production, spatial distribution of heat deposition, radioactive inventory, among others have to be correctly estimated to avoid failure or poor performance of the targets. This is an on-going activity that is expected to grow as the design activities of RIA evolve.

c.4. Implementation of Photonuclear and Low Energy D-Li Capabilities for Target Design (I. C. Gomes and J. A. Nolen)

The capability of performing photonuclear analysis in ISOL type targets was implemented and tested at the NERSC and Physics Division computers. A set of photonuclear cross section data and the compatible MCNPX code was implemented and tested. The remarkable forwarded peaked distribution of photons created by the interaction of an electron beam with a heavy element target presents some attractive features for ISOL type of applications. The photonuclear cross section library was obtained directly from Dr. MacFarlane (Los Alamos National Laboratory) and it is a revised version of all photonuclear libraries created by an IAEA workgroup that included many countries. The cross section library is compatible with the MCNPX photonuclear capability and contains data for photofission of a few isotopes. The applicability of a 45-MeV electron beam hitting a 2.5-g/cm^3 uranium carbide target for rare isotopes production was analyzed. The advantage that this system provides is the highly concentrated fission distribution. However, while the compactness of the target is a highly desirable feature, problems derived from the heat deposition profile seem to impose a difficult hurdle for this approach. Figure III-27 displays the fission distribution profile for a 500-μA electron beam with 45 MeV of energy hitting directly a solid uranium carbide cylinder with 2.5-g/cm^3 density. The fission rates were multiplied by the volume of the each ring to provide a more realistic picture of the importance of each target region on the total fission production.

Another implementation was to introduce in the MCNPX code a double-differential cross section set for the deuteron-lithium interaction. The cross section data was introduced into the source routine of the code in such a way that neutron production by the interaction of deuterons with energy up-to 40 MeV with a lithium target can be simulated. The advantage of using MCNPX is that the nuclear models included in the code allow a more realistic transport analysis of neutrons generated with energy above 20 MeV. Figure III-28 displays the fission distribution inside of a 2.5-g/cm^3 uranium carbide target irradiated by neutrons produced from the interaction of a 5-mA beam of 40-MeV deuterons with a lithium jet. The fission rate was multiplied by the volume of the ring providing a better

picture of the importance of each radial position of the target regarding fission production. It can be noticed that the fission production spreads across the target much more than the photon fission of Fig. III-27. However the total fission generation and the heat deposition profile are more favorable than the electron-beam case.

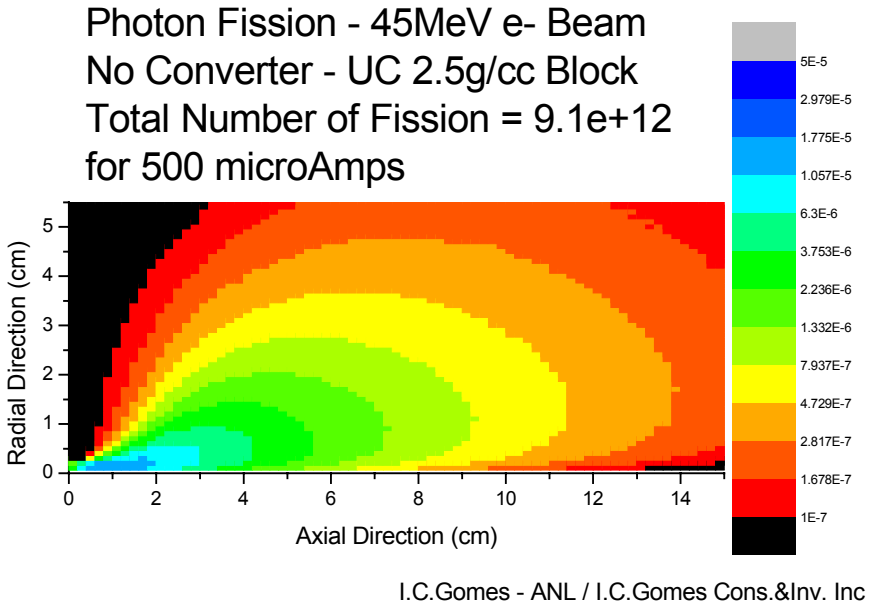

Fig. III-27. Fission Distribution profile for a 45MeV electron beam hitting a 2.5g/cm^3 UC target. The fission rates are multiplied by the volume of the ring segment represented by each cell of the geometric configuration.

.

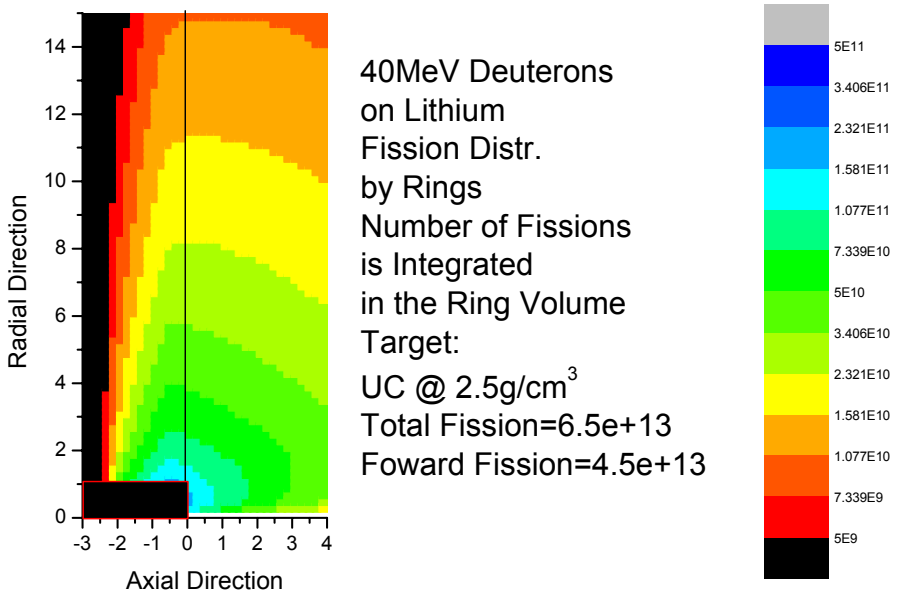

Fig. III-28. Fission Distribution profile for a 40-MeV, 5-mA deuteron beam hitting a lithium target. The produced neutrons induce fission in a 2.5g/cm^3 UC secondary target. The fission rates are multiplied by the volume of the ring segment represented by each cell of the geometric configuration.

c.5. Effusion/Diffusion Studies of ISOL Target/Ion Source Systems (B. Mustapha, J.A. Nolen, J.-C. Bilheux,* and G.D. Alton*)

In previous studies, we have shown that it is possible to characterize the release process and extract its important parameters by comparing simulated release curves to the experimental ones measured with a given target geometry for a given isotope. The extracted information can then be used to improve the efficiency of existing targets and design new geometries more suitable to produce beams of rare isotopes. We report here on a more thorough study of the RIST target[1] and on the progress of the simulation of the ORNL target/ion source system used to measure effusion times of rare gases.[2]

RIST Target

A thorough study of the RIST target[3] has shown that the diffusion coefficient (D) can not be determined when the decay of the considered isotope is faster than its diffusion through the target material, which is the case of most short lived isotopes. In this case data from the closest long-lived isotope can be used. For ^{8}Li the best fit to the data was obtained for D=10^{-8} cm^2/s (measured for ^{7}Li [Ref. 4] and a sticking time ts=0 ns, but the data seems to be slightly faster than the simulation. In order to understand this discrepancy, two possible effects have been examined; first, a non uniform target temperature and second, an electric field in the ionizer. The non-uniform temperature was simulated by adding a faster diffusion component and the electric field by shortening the ionizer length. A quite good fit was obtained by considering a 0.9 % contribution from a faster diffusion with D=10^{-5} cm^2/s, see Fig. III-29. A better fit was obtained, however, with a 2-cm ionizer length instead of the original 3.5-cm length, see Fig. III-30. To decide which effect is really acting (it could be both), dedicated measurements are needed.

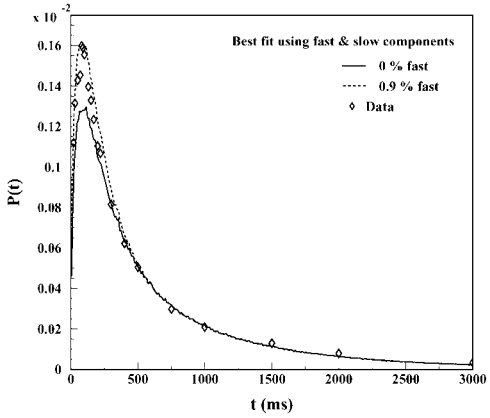

Fig. III-29. Best fit by considering a fast diffusion component.

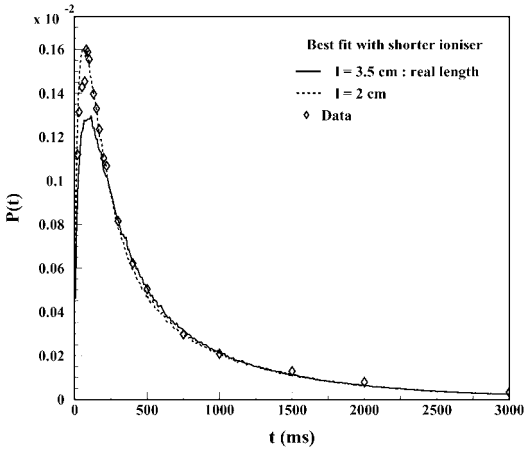

Fig. III-30. Best fit by shortening the ionizer.

ORNL Target/Ion Source systems

To better characterize the diffusion and effusion processes and avoid the uncertainty coming from the indertermination of D, we propose here to deconvolute the two processes and study them separately (the release process is the convolution of the diffusion and effusion processes). We report here on the progress of the simulation of Target/Ion Source systems used at Oak Ridge National Laboratory (ORNL)[2] to measure effusion times of some rare gases. Two different target geometries have been used at ORNL to measure effusion times of He, Ne, Ar, Xe and Kr at different temperatures. Data have been taken for both an empty target chamber and one filled with a Reticulated Vitreous Carbon Foam (RVCF) matrix.

We have implemented the geometry of their first system (serial coupling) for the empty target case and run the effusion part of the calculation. Figure III-31 shows the corresponding geometry and the track of one particle. The target tube is 19.3 cm long and 1.5 cm diameter. The connecting tube is about 10 cm long and 7.5 mm diameter coupling the target to an Electron Beam Plasma Ion Source (EBPIS). The output of the calculation is a number of collisions and a total path length for each event. We have found that on the average particles bounce 3000 times and travel about 24 m before exit the ion source. This output can be used to determine the effusion time for any isotope through the same system at any temperature.

The comparison of the simulation to the experimental data is in progress. This step is important to benchmark the effusion part of the calculation. Future studies of more reactive gases will permit the determination of sticking times for various gas and material combinations.

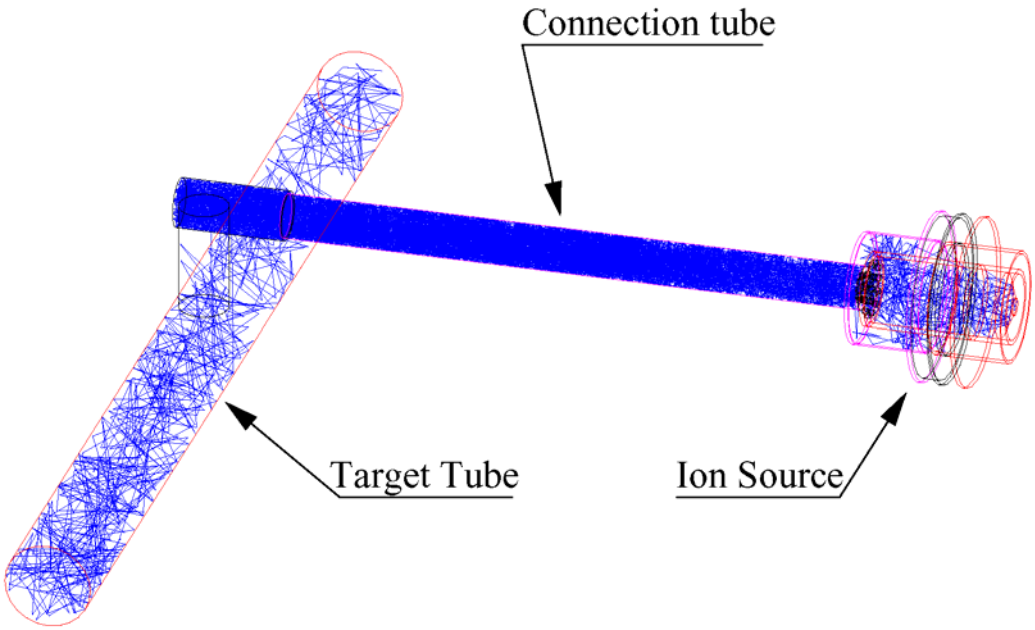

Figure III-31. Geometry of the first Target/Ion Source system (serial coupling) used at ORNL showing the track of one particle.

*Oak Ridge National Laboratory

[1]J. R. J. Bennett et al, NIM B 126 (1997) 117.
[2]J. C. Bilheux and G. D. Alton et al, Proceedings of the 2001 Particle Accelerator Conference, Chicago.
[3]B. Mustapha and J. A. Nolen, EMIS-14 proceeding, to be published in Nuclear Instruments & Methods B.
[4]J. R. J. Bennett, private communication.

c.6. An Adjustable Thickness Li/Be Target for Fragmentation of 4-Kw Heavy-Ion Beams

(J.A. Nolen, C.B. Reed,* A. Hassanein,† V. J. Novick,* P. Plotkin,* J.R. Specht, D.J. Morrissey,‡ J.H. Ottarson,‡ and B.M. Sherrill‡)

The need for a thick windowless liquid lithium target for use with high intensity uranium beams at next-generation radioactive beam facilities has been discussed.[1,2] Lighter heavy ions at such high energy fragmentation facilities require thicker targets, in the 5-10 g/cm^2 range, which corresponds to 10-20 cm in thickness if pure lithium is used. Since the density of beryllium is about 4 times that of lithium, a hybrid target using both lithium and beryllium was proposed.[2] A first-generation target of this type, for use with beam power of up to 4 kW, is currently under construction for use with beams from oxygen to calcium at the NSCL A1900 fragment separator.[3] A schematic layout of this target concept is shown in Fig. III-32. The design of this target, which covers a thickness range from 0.7 to 3 g/cm^2, is described in this paper.

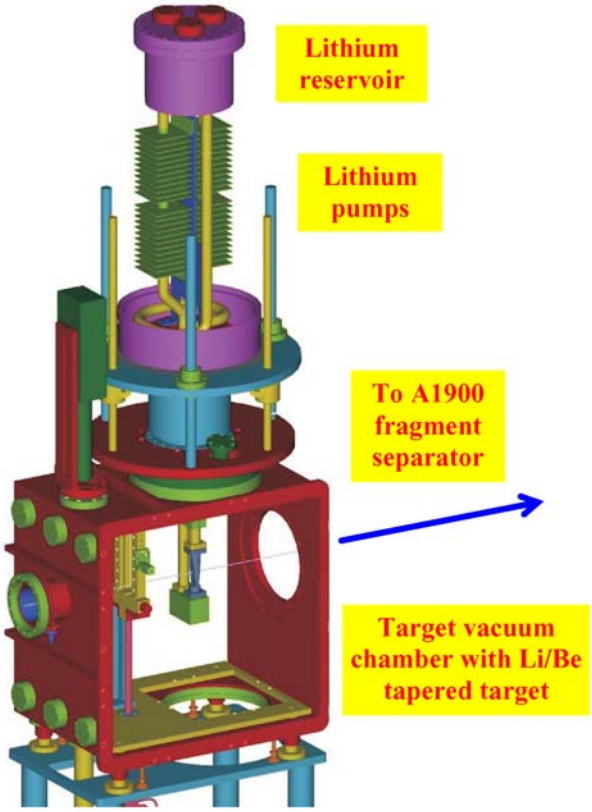

Fig. III-32. A schematic view of the target chamber at the NSCL A1900 fragment separator. The chamber is designed to accommodate the liquid lithium loop from above and a standard target ladder from below. The containment vessel is removed in this view.

At high energies there is relatively little influence of the target material on the distribution of produced fragments. In this case, low-Z target materials are preferred since the overall production rate is larger. Beryllium and graphite have been used extensively at existing fragmentation facilities. Lithium is also an appropriate choice for target material and, as discussed previously, is also an excellent cooling medium. A combination of beryllium and liquid lithium can be used to limit the total linear target thickness to reasonable values. At the NSCL after the recently completed Coupled Cyclotron Upgrade,[3] the most powerful beams are in the mass range between oxygen and calcium where beam power up to 4 kW is possible. For these beams a target thickness over the range from 0.7 to 3 g/cm^2 is a good match to the acceptance of the A1900. The hybrid-target spool piece designed to cover this thickness range is shown schematically in Fig. III-33.

Fig. III-33. A cutaway view of the beryllium target spool piece for the hybrid target. The beryllium entrance and exit windows vary from 1-mm thick at one end to 7-mm thick at the other. Lithium flows between the windows and is 5 mm thick. The overall target varies from 0.7 g/cm^2 to 3 g/cm^2.

Three-dimensional thermal calculations of the temperature profiles in the entrance and exit regions of the target have been carried out using the HEIGHTS simulation program.[4] The results of the simulations done for a ^{48}Ca beam at 160 MeV/u and 0.5 particle microampres at the thin end of the target (1-mm beryllium windows and 5-mm lithium thickness) are shown in Fig. III-34. Corresponding results for an ^{16}O beam at 200 MeV/u and 1.0 particle microamperes at the thick end (7-mm beryllium windows and 5-mm lithium) are shown in Fig. III-35. For these calculations a heat transfer coefficient of 20 W/cm^2-K was used for the liquid lithium flowing at a velocity of 4 m/s.

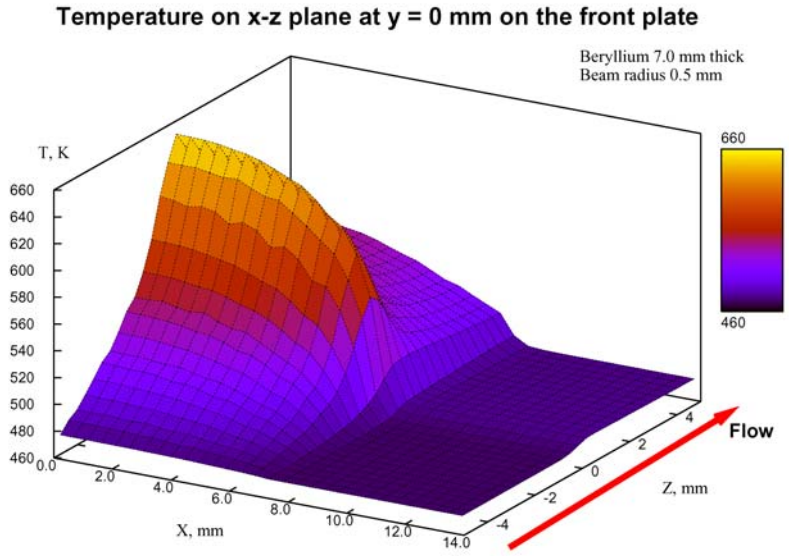

Fig. III-34. Three-dimensional thermal calculation of the temperature distribution in the beryllium window and flowing lithium for the case of a 200 MeV/u ^{16}O beam at an intensity of 1 particle microampere. The peak temperature is at the outside surface of the beryllium and is 660 K.

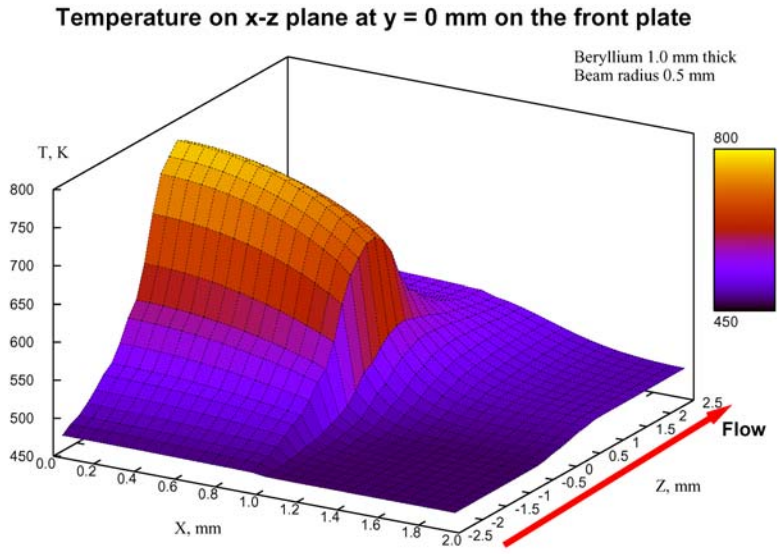

Fig. III-35. Three-dimensional thermal calculation of the temperature distribution in the beryllium window and flowing lithium for the case of a 160 MeV/u ^{48}Ca beam at an intensity of 0.5 particle microampere. The peak temperature is at the outside surface of the beryllium and is 800 K.

Pressure/flow requirements and pump design

The approximately 1-kW power dissipation in the target implies that only a relatively low volume flow rate, ~4 m/s, is required to keep the peak temperature rise in the lithium to about 100 °C. With a channel cross section of 5 mm by 10 mm in the target spool piece, the pressure drop across the target is only ~3000 Pascals. The liquid-lithium pump design and the pipe sizing of the lithium loop were chosen to be compatible with this target flow rate and pressure drop.

A DC, permanent magnet Lorenz-force type of pump was chosen for this application. This type and other liquid metal pumps are reviewed in a NASA report.[5] Because of the operating temperature of ~200 °C, Sm_2Co_{17} permanent magnet material is being used for the pump. This material is also ~1000 times more radiation resistant than NdFeB permanent magnet materials.[6,7] A prototype pump has been built and tested using a Ga/In alloy that is liquid at room temperature. A schematic of the present pump design is shown in Fig. III-36. It is a smaller and simpler version of a liquid gallium pump developed by Smither.[8]

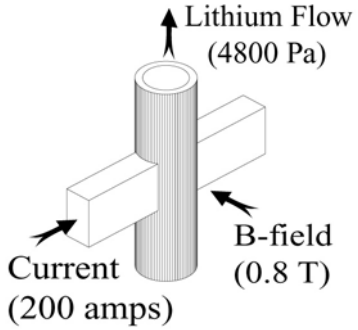

Fig. III-36. Schematic diagram of the permanent-magnet, liquid-lithium pump. The pump is designed to deliver a volume flow rate of 200 cm^3/s at the pressure, current, and magnetic field indicated. With these parameters and the piping as designed, the flow velocity through the target spool piece is 4 m/s and the pump voltage is 24 mV. The no-flow voltage is 10 mV. The stainless steel tube through the pump is 12.7 mm outside diameter and the wall thickness is 1.6 mm.

Mechanical layout

The target assembly, liquid-lithium loop, lithium pump, and associated heaters and temperature monitors comprise an assembly that mounts on the top flange of the target vacuum chamber of the NSCL A1900 fragment separator and is compatible with the standard target ladder. The operating temperature of the liquid-lithium loop is 200 °C so that the heater control system will have to adjust the heater power as required by the amount of beam power being dissipated in the target. A mechanical assembly drawing of the overall target system is shown in Fig. III-37. A detailed system design description is given in [Ref. 9].

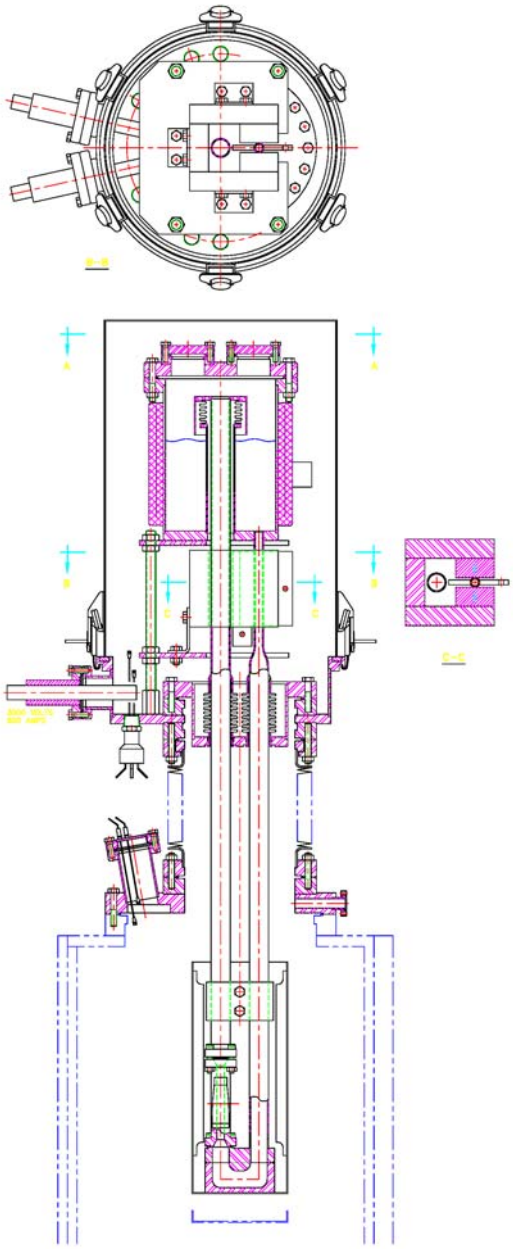

Fig. III-37. Drawing of the mechanical layout of the liquid-lithium loop. The mechanism can move vertically with respect to the beam in order to vary the target thickness or to withdraw the mechanism to make room for the standard target ladder. A section view of the permanent-magnet pump is shown to the right.

Safety issues and procedures

One of the goals of this project is to develop procedures for the safe operation of liquid-lithium target systems at a radioactive beam facility. The general safety issues associated with liquid alkalis were discussed at RNB-5.[1] Such procedures have been developed and used in fusion research programs and liquid-metal cooled reactors. The present target uses a closed lithium loop, which is an intermediate step towards the operation of a windowless target at a nuclear physics accelerator facility. However, to provide an additional measure of isolation of the liquid lithium from the laboratory environment, the present design incorporates a secondary containment vessel as shown in Fig. III-37, as well as, a pressure relief valve for the inert cover gas above the lithium in the closed loop.

Construction and testing schedule

The design of this prototype target is complete and fabrication is in progress. The DC pump has been constructed and the beryllium spool piece has been procured. The present plan is to complete fabrication of the target system at the NSCL in the fall of 2002, and to assemble and test it, without beam, at Argonne soon thereafter. It should be ready for commissioning at the NSCL A1900 in 2003.

*Technology Development Division, Argonne National Laboratory
†Energy Technology Division, Argonne National Laboratory
‡Michigan State University

[1]J.A. Nolen, C.B. Reed, A. Hassanein, and I.C. Gomes, Nucl. Phys. **A701** (2002) 312c-322c.
[2]J.A. Nolen, et al., abstract #78, EMIS-14.
[3]D.J. Morrissey, abstract #70, EMIS-14.
[4]A. Hassanein and I. Konkashbaev, J. Nucl. Mater. **273** (1999) 326.
[5]J.P. Verkamp and R.G. Rhudy, "Electromagnetic Alkali Metal Pump Research Program," NASA Contractor Report CR-380, Feb. 1966.
[6]A.F. Zeller and J.A. Nolen, 9th Int. Workshop on Permanent Magnets, Bad Sodem, FRG, (1987) 159.
[7]O.-P. Kähkönen, et al., Phys. Rev. **B49** (1994) 6052-6057.
[8]R.K. Smither, "Summary of the Operating Characteristics of the ANL Liquid Metal Pump after its Latest Modification, APS Technical Memo: AGP-III-M, September 20, 1995.
[9]"System Design Description for the ANL/MSU Li/Be Target Loop," ANL/TD document G0586-0003-SA, July 2002.

c.7. Development and Operation of Gas Catchers to Thermalize Fusion-Evaporation and Fragmentation Products

(G. Savard,* J. Clark,† C. Boudreau,‡ F. Buchinger,‡ J.E. Crawford,‡ S. Gulick,‡ A. Heinz,* J.K.P. Lee,† A. Levand,* D. Seweryniak,* K.S. Sharma,† G. Sprouse,§ J. Vaz,† J.C. Wang,† B.J. Zabransky,* Z. Zhou* and the S258 collaboration)

A new approach to the production of low energy radioactive beams involves the stopping of fast beams produced by fragmentation, in-flight fission or fusion-evaporation reactions into a large gas catcher where the reaction products are thermalized in high-purity helium and extracted as singly charged ions for post-acceleration. This removes the limitation present in standard ISOL technique for species that are difficult to extract from the target/ion source assembly. This approach has been implemented at Argonne since 1998 to inject fusion-evaporation products in an ion trap system. Via a series of improvements since then, we now reach efficiencies for these devices of close to 50% with delay times below 10 ms. In preparation for the RIA project, a larger device for stopping fragmentation products has been designed and is currently under construction. Preparation for a test of this large gas cell at the full RIA energy at GSI is also in progress.

A large gas catcher system was first developed at Argonne in 1998 for the injection of radioactive ions into the CPT mass spectrometer.[1] It used a large high-purity helium gas volume where fast reaction products separated by a gas filled spectrograph were stopped and thermalized as 1+ ions before being extracted from the

catcher. For high-efficiency, the gas catchers must have a stopping volume large enough to contain the full range straggling of the reaction products in which case the gas flow alone (as in a typical IGISOL[2] system) cannot extract the ions quickly enough. The ion extraction is therefore assisted by electric DC and RF fields applied in the high-pressure catcher to pull out the ions faster than the gas itself is evacuated. We proposed at that time that this technique could be extended to the stopping of fragmentation products which led to an important new production mechanism for the proposed RIA[3] facility.

In the years of operation of the fusion-evaporation gas catcher system at ATLAS, this technology have been developed and tested over a series of prototype, and extraction efficiencies of 45% with delay times below 10 ms are now reached, both of those with space-charge density inside the gas catcher typical of on-line operation. In particular, we have recently investigated the space-charge density that such devices can tolerate while maintaining high efficiency. This effect will ultimately limit the yield that can be extracted from such devices in large facilities like RIA. Finally, in preparation for the RIA project, we are now extending this work with the design and construction of a 1.25 meter long gas cell for stopping fragmentation product. This full scale RIA prototype will be characterized at Argonne before being installed on-line behind the FRS separator at GSI to demonstrate that this approach is valid even for very high-energy reaction products.

The gas catcher currently being used for stopping of fusion-evaporation products has an inner diameter of about 8 cm and a length of roughly 27 cm, and uses only UHV materials. It is installed at the focal plane of an Enge spectrograph. It is separated from the spectrograph vacuum chamber by an all metal 1.9 mg/cm^2 HAVAR window sealed by indium rings and supported by a gold coated tungsten wire grid. The cell is filled with ultra-high-purity helium gas fed by an all stainless steel gas system, with the gas purified by a Monotorr purifier (SAES getters Inc.) preceded by a standard cold trap. This catcher delivers the extracted ions into a 3 section RFQ gas cooler where the flowing helium gas is pumped away in the first section by clean booster pumps backed by a roots blower. Diagnostics for ions (counting and mass selectivity) and radioactivity is provided after the gas cooler. The gas catcher has DC fields guiding the positive ions towards the extraction region where an RF-focusing cone (Fig. III-38) focuses the ions on the 1.6-mm diameter extraction nozzle. The focusing force is essentially an RF wall which keeps the ions away from the cone. The repulsive force depends on the mobility of the ions in the gas and decreases with higher gas pressure. The RF cone used in the fusion-evaporation gas catcher has been operated successfully up to the maximum pressure the thin window to let the recoils enter the catcher can tolerate, which is about 250 mbar. The efficiencies and extraction times measured with the device are shown in Fig. III-39.

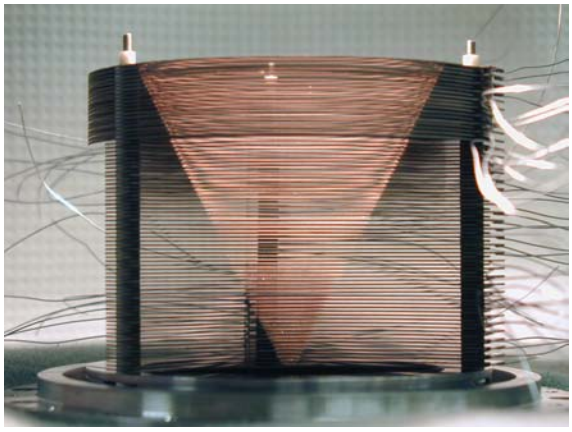

Fig. III-38. Conical RF structure used to focus the ions on the extraction nozzle of the gas catcher.

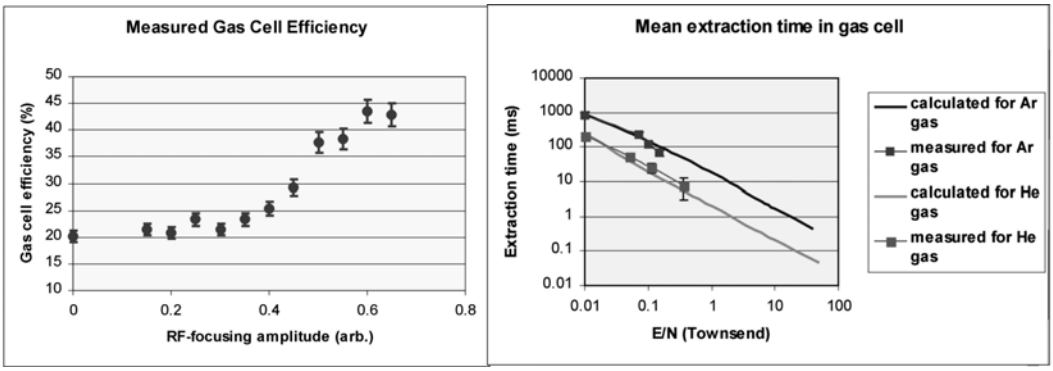

Figure III-39: Measured efficiency and mean extraction time as a function of RF and DC fields applied inside the gas catcher.

A number of systematic studies have been performed with the gas catcher system, looking at the effect of impurities in the gas, gas flow conditions, transmission through the cooler system, efficiency variation with DC and RF parameters inside the catcher, etc. While these studies are still ongoing, a few conclusions can already be drawn. The most important conclusion is that the effect of impurities in the gas reduces significantly as the field gradient inside the cell is increased. It appears that the long-range attraction of the ions and impurities does not succeed in bringing together ion and impurity molecules in the presence of the constant collisions which the molecule must undergo to "follow" the ion being dragged in the helium gas. Similarly, the adducts of ion plus helium which are weakly bound are not observed when the electric field becomes significant. Under optimal conditions we find no sign of activity at masses other than those of the radioactive ions being produced.

The device then underwent a series of tests to determine the dependence of the method on the chemical properties of the extracted ions. The basis of the argument for chemical independence is that all species have much lower ionization potential than helium so that they will remain ionized after the deceleration process. The presence of impurities in the gas might however still lead to losses for the most chemically active ions. We have produced a series of radioactive ions of different species and looked at their behavior as impurities are introduced in the ppb level purity gas available at the area II spectrograph. We have found that with sufficiently large accelerating fields inside the cell the system is quite insensitive to sub-ppm level contaminants and have even found a surprisingly large surviving fraction of 2+ ions extracted for some species.

In on-line studies, we have created radioactive species and brought them into the cell together with a fraction of the primary beam. This fraction can be varied by tuning the dispersion of a velocity filter[4] that has been added at the entrance of the Enge spectrograph. While these studies are still coarse, we do observe saturation effects in the cell which occur at a rate consistent with that we predicted for the point where charge accumulation in the cell will shield the electric field applied. In these tests, the gas catcher has been operated with high efficiency at ionization densities in excess of 10^8 ion-electron pairs created per cm^3 per second, well above the maximum level predicted by a simple model in the literature.[5] This number is therefore consistent, when scaled to a cell of the size required for RIA, with the roughly 10^9 ions per second limit we expect to be able to handle with this approach at RIA and which was used for the RIA yield calculations[6] using this extraction system.

The next step in the gas cell evolution is a full scale RIA gas catcher prototype that will be tested with heavy beams at the full RIA energy which are available at GSI. The characteristics of the large gas cell system required for the high-energy test were developed from an analysis of the beam properties available at the FRS at GSI and of the recoil achromatization system that will be used. The ±1% momentum acceptance and 10 mrad angular acceptance of the FRS, together with the 7cm/% momentum dispersion that will be used for the achromatization of the beam and the angular straggling in the final degrader and the lateral straggling in the gas cell itself determine a stopping width of about 20 cm for the recoils. The longitudinal range straggling can be compressed by the achromatization by a factor of 10 or so as has been shown experimentally at the FRS.[7] This yields the 0.5 atmosphere-meter of helium stopping length required. We have therefore designed the body of the cell that will mate to a large conical extraction

region to have a stopping volume with an inner diameter of 25 cm and a total length of about 1.2 meters. It is a scaled up version of the gas cell bodies developed for the CPT at Argonne. Because of the large surface area and the low pumping speed it is important to use only UHV techniques in the design and construction of the cell and the body and the inner rings and insulators are therefore constructed with only stainless steel, aluminum oxide, aluminum and indium seals (see Fig. III-40). The mechanical construction of the full scale RIA gas cell prototype has been ongoing since the end of FY2001. Final assembly of the full gas cell vacuum system with all its inner electrodes, about 7300 components with over 4000 components cleaned to UHV standards, is being completed (Fig. III-40). Construction of all tuned circuits for the different RF focusing electrodes and the DC gradient is ongoing, together with the connection to the gas cooler and basic diagnostics for slow ions. The full system will be surrounded by a high-voltage protection cage and will form a movable unit that can easily be moved to different locations. This system will be first tested off-line with a fission source before on-going characterization on-line with low-energy radioactive species produced on-line at Argonne. Using the high-quality beams of ATLAS, thin production targets and a tunable degrader assembly, radioactive isotopes will be deposited at well-defined locations inside the cell. This will allow the efficiency to be determined as a function of position inside the cell. Pulsing the ATLAS beam on a slow time cycle (typically a half a second or so) will allow us to also determine the extraction delay times as a function of position inside the cell. Effect of space-charge saturation will also be investigated as a function of pressure inside the device. After these tests the device will be moved to GSI for operation behind the FRS where site preparation involving a large international collaboration (experiment S258: Argonne, GSI, Jyvaskyla, Leuven, Giessen, Muenchen, Michigan State, Stony Brook and RIKEN) is ongoing.

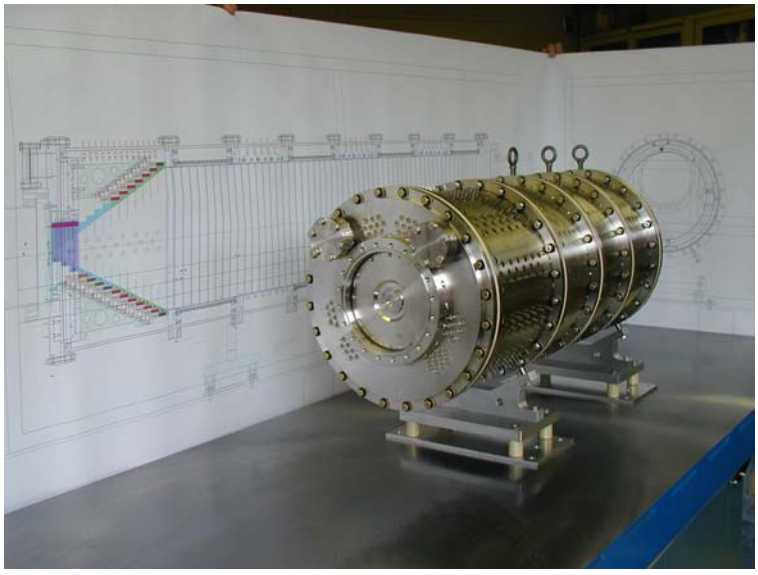

Figure III-40: View of the large gas catcher being developed for testing at the FRS.

[*]Physics Division, Argonne National Laboratory, Argonne, IL 60439
[†]Department of Physics and Astronomy, University of Manitoba, Winnipeg, MB R3T 2N2
[‡]Department of Physics, McGill University, Montreal, PQ H3A 2T8
[§]Physics Department, SUNY, Stony Brook University, Stony Brook, NY 11794

[1]G. Savard, R.C. Barber, C. Boudreau, F. Buchinger, J. Caggiano, J. Clark, J.E. Crawford, H. Fukutani, S. Gulick, J.C. Hardy, A. Heinz, J.K.P. Lee, R.B. Moore, K.S. Sharma, J. Schwartz, D. Seweryniak, G.D. Sprouse, J.Vaz, Hyperfine Interactions 132 (2001) 223.
[2]P. Dendooven , Nucl. Instr. Meth. B126 (1997) 182.
[3]G. Savard, in *Proceedings of the 2001 Particle Accelerator Conference*, Chicago, Illinois, 2001, edited by P. Lucas and S. Webber (IEEE, Piscataway, NJ, 2001), p.561.
[4]J. Clark et al, "Improvements in the injection system of the Canadian Penning Trap mass spectrometer", EMIS-14

[5]M. Huyse et al, "Intensity limitations of a gas cell for stopping, storing and guiding of radioactive ions", submitted to NIM B.
[6]C.-L. Jiang et al, "Yield calculations for a facility for short-lived nuclear beams", submitted to NIM B, also available at http://www.phy.anl.gov/RIA/.
[7]C. Scheidenberger et al, "Energy and Range focusing of in-flight separated exotic nuclei – a study for the energy-buncher stage of the low-energy branch of the Super-FRS", EMIS-14 proceedings.